RESEARCH ACTIVITIES VIII
Computer Center

VIII-A Theoretical Studies on Electronic Structure and Dynamics of Electronically Excited States in Polyatomic Molecules

VIII-A-1 Wavepacket Study on the Photodissociation Dynamics of OCS

Toshinori SUZUKI, Hideki KATAYANAGI, Shinkoh NANBU and Mutsumi AOYAGI

[*J. Chem. Phys.* **109**, 6838(1998)]

Prof. Suzuki's experimental group has measured the speed, angular and alignment distributions of $S(^1D_2)$ atoms from the ultraviolet photodissociation of OCS by a photofragment imaging technique. It was found that the dissociation from A' state gives rise to high- and low-speed fragments, while the A" state only provides the high-speed fragment. In order to elucidate the dissociation dynamics, in particular the bimodal speed distribution of S atoms, two-dimensional potential surfaces of OCS were calculated for the C-S stretch and bending coordinates by ab initio State-Averaged CASSCF/MRSDCI method. Conical intersections of $^1\Delta$ and $^1\sum^-$ with $^1\prod$ were found as adiabatic dissociation pathways. Wave packet calculations on these adiabatic surfaces, however, did not reproduce the low-speed component of the $S(^1D_2)$ fragments. The discrepancy regarding the slow S atoms was attributed to the dissociation induced by non-adiabatic transition from $2A'(^1\Delta)$ to $1A'(^1\sum^-)$ in the bending coordinate. This was confirmed by wave packet calculations including non-adiabatic transitions. The slow recoil speed of S atom in the non-adiabatic dissociation channel is due to more efficient conversion of bending energy into CO rotation than the adiabatic dissociation on the upper surface.

VIII-A-2 Theoretical Study on the Predissociation Dynamics of Electronically Excited $^1\Delta$ state of HCP Molecule

Shinkoh NANBU, Tomoko KINOSHITA and Mutsumi AOYAGI

The potential energy surfaces and transition dipole moment surfaces of the low-lying electronically excited states of HCP molecule are calculated using the ab initio state averaged CASSCF and multi reference configuration interaction (CI) method. The photodissociation dynamics for $HCP(1^1\sum^+) + h\nu \rightarrow H(^2S) + CP(X)$; where $X = 1^2\sum^+$ and $2^2\prod$, are investigated by performing wave packet calculations on ab initio surfaces. The photoabsorption cross section of HCP $(1^1\sum^+) + h\nu$ (299-237nm) and the rovibrational state distribution of the CP product were evaluated. We found that the non-adiabatic transition between $1^1A'$ and $2^1A'$ states in the bent conformations plays an important role in the predissociation process.

VIII-A-3 Theoretical Study on the Unimolecular Reaction Dynamics of Acetyl Radical $CH_3CO \rightarrow CH_3 + CO$

Masakatsu ITO, Shinkoh NANBU and Mutsumi AOYAGI

Prof. Suzuki's group at IMS has shown that the RRKM unimolecular dissociation rate constant k(E) of internally excited acetyl radical did not reproduce the experimental values. We investigate the dissociation dynamics of acetyl radical with the classical trajectory method using the electronic model hamiltonian based on our ab initio calculations. At each time step in our classical trajectory calculations, the electronic hamiltonian is diagonalized to obtain the instantaneous adiabatic states and then the Hellmann-Feynmann forces are evaluated to drive the nuclear coordinates. Our hamitonian is based on the valence bond (VB) description of the electronic wavefunctions. Since acetyl radical and its dissociative products have completely different bonding characters, the wavefunctions along the dissociation process are approximately expanded by two correponding VB bases states.

UHF/MP2/6-311G** calculations at various nuclear conformations are carried out to fit the potential parameters in the model hamiltonian. The maximum deviation of the model potential energies from the ab-initio ones is 0.0038 hartree, which is about one-tenth of the barrier height. Although this level of calculation is accurate enough to describe the qualitative characters in dissociation processes of acetyl radical, the resulting barrier height is still 4 kcal/mol heigher than the experimentally proposed value. Hence we modified two parameters from the PUHF/MP4/6-311G** calculations, where barrier height is as accurate as the experimental value(15 kcal/mol).

The initial preparations of the trajectories are employed with a Monte Carlo "random walk" in conformational space for microcanonical sampling. We found that the energy of the CCO bending excitation does not efficiently transfer into the dissociation coordinate(C-C) over the time period of 30 ps. We suggested that this slow transfer or redistribution of internal energy could be one of the important sources for the discrepancy between the RRKM rate constants and the experimental values. We continue to analyze the detailed IVR processes of internally excited acetyl radical to clarify the reason for experimentally observed non-RRKM behavior.

VIII-A-4 Ab Initio Molecular Orbital Studies of Isomerization Reaction from c-$OSiH_2O$ to t-

OSiHOH

Shigeo KONDO *(Nat. Inst. of Material and Chemical Research)*, **Kazuaki TOKUHASHI** *(Nat. Inst. of Material and Chemical Research)*, **Hidekazu NAGAI** *(Nat. Inst. of Material and Chemical Research)*, **Akifumi TAKAHASHI** *(Nat. Inst. of Material and Chemical Research)* **and Mutsumi AOYAGI**

[*J. Mol. Struct. (THEOCHEM)* in press]

We have suggested in a previous study that the reaction route from $SiH_3 + O_2$ to OSiOH + 2H is a key to understand the spontaneous ignition at room temperature. The whole route of this reaction was found as follows;

$SiH_3 + O_2 \rightarrow$ SiH3OO*
$\rightarrow$ c-$OSiH_2O$ + H
$\rightarrow$ OSiHOH + H
$\rightarrow$ OSiOH + 2H

In this study, we investigated the detailed isomerization mechanism from c-$OSiH_2O$ to t-OSiHOH with *ab initio* Gaussian-2 theory and CASSCF(6,6) method. It was found that the reaction proceeds through two consecutive steps; i.e., c-$OSiH_2O$ undergoes isomerization to yield w-$OSiH_2O$, and then the latter is converted to t-OSiHOH. The G-2 energy of the transition state of the latter process is 4.3 kcal/mol higher than that of the former. However, the G-2 energy of this higher transition state plus H atom is still 4.8 kcal/mol lower than that of the original reactants of $SiH_3 + O_2$.

VIII-A-5 Ab Initio Study of $PH_2 + O_2$ Reaction Relevant to the PH_3 Combustion

Shigeo KONDO *(Nat. Inst. of Material and Chemical Research)*, **Kazuaki TOKUHASHI** *(Nat. Inst. of Material and Chemical Research)*, **Akifumi TAKAHASHI** *(Nat. Inst. of Material and Chemical Research)*, **Masaaki SUGIE** *(Nat. Inst. of Material and Chemical Research)* **and Mutsumi AOYAGI**

[*J. Phys. Chem.* submitted]

Ab initio calculations have been carried out for the $PH_2 + O_2$ reaction by using Gaussian-2 theory, which is considered as a key reaction to understand low temperature phosphine combustion. This reaction consists of two main branching routes at low temperatures. One is the reaction to yield OH radicals, and the other to yield hydrogen atoms, Of the two reactions, we found that a long reaction pathway;

$PH_2 + O_2 \rightarrow PH_2OO$
$\rightarrow$ c-OPH_2O
$\rightarrow$ w-OPH_2O
$\rightarrow$ OPHO + H
$\rightarrow$ OPO + 2H

has been concluded to be the chain branching process, which enables the spontaneous ignition of phosphine at room temperature.

VIII-A-6 Semiclassical Study of Nonintegrable Systems

Toshiya TAKAMI

We study nonadiabatic process in classically nonintegrable systems such as 2D billiards and kicked rotators to reveal essence of the dynamical characters in the highly excited states of molecules. Nonadiabatic transition between adjacent levels through an avoided crossing was studied first in pioneering works by Landau, Zener, etc. In the nonintegrable systems, however, Landau-Zener formula cannot be applied because the system contains essentially many levels and nonadiabatic couplings between adiabatic states are not vanish everywhere.

On the numerical experiments of nonintegrable systems, we found non-Landau-Zener behavior in the nonadiabatic process, and we pointed that this phenomenon arises from a boundary term which is missed in Landau-Zener formula. Applying this extra term, we construct new basis functions which can describe nonadiabatic transition locally even in many level systems. We use semiclassical methods to obtain the new basis and to study physical properties of them.

VIII-A-7 A Theoretical Study on Structures and Vibrational Spectra of C_{84} Fullerene Isomers

Takeshi NISHIKAWA, Tomoko KINOSHITA, Shinkoh NANBU and Mutsumi AOYAGI

[*J. Mol. Struct. (THEOCHEM)* in press]

The C_2, D_2, and D_{2d} isomers of C_{84} fullerene were investigated by ab initio molecular orbital calculations. Optimized geometries, relative stabilities, and vibrational spectra of eleven isomers are determined by restricted Hartree-Fock (RHF) calculations with STO-3G, 3-21G, and D95V basis sets. For the purpose of an assignment on the C_{84} structures, we discussed a way to distinguish a specific isomer by comparing the calculated vibrational spectra.

We found that the peaks located at higher than 1300 cm^{-1} are all belonging to the on-surface mode where each carbon atom moves on the surface of C_{84} skeleton. On the other hand, the peaks below 1000 cm^{-1} correspond to the breathing mode, in which atoms are moving perpendicularly to the surface. There exists a window region(around 1000-1300 cm^{-1}) in all calculated spectra, which split a character of normal mode vibrations. In D_2 symmetry, the vibrational spectra of isomer No. 1 has a noticeable difference in the locations of three main peaks. The isomer No. 2 with C_2 symmetry also has characteristic vibrational structure, where numbering scheme introduced by Fowler et. al. is used. For the rest of other isomers examined, it was hard to clearly predict the structure solely with calculated vibrational spectra. We suggested that the difference in the bands around 650 cm^{-1} and 1670 cm^{-1} can be used as a finger print of D_2

isomers, and that the vibrational bands below 900 cm^{-1} and peak around 1880 cm^{-1} can be used to distinguish C_2 species.

Laser Research Center for Molecular Science

VIII-B Zero Kinetic Energy Pulsed Field Ionization Spectroscopy of Very Highly Excited Rydberg States and van der Waals Complexes

Zero kinetic energy pulsed field ionization (ZEKE-PFI) spectroscopy is a very high resolution (~0.1 meV) photoelectron spectroscopic technique based on PFI of very highly excited Rydberg states. The very highly excited (n > 100) Rydberg states, which have unexpectedly long lifetimes, are investigated with a newly developed two-pulsed field ionization technique. The van der Waals complexes of aromatic compounds with rare gas atoms are also studied to clarify inter-molecular forces of cationic vdW complexes.

VIII-B-1 Energy Exchange between Electron and Ion Core in Very High-Lying Rydberg States of Poliatomic Molecules Evidenced by Sweep-Off-Probe Pulsed-Electric-Field Ionization

Shin-ichiro SATO, Yoshitaka NOZAKI *(Sigma Kouki Co.)* **and Katsumi KIMURA**

We have newly developed the Sweep-off-Probe Pulsed-Field Ionization (SOP-PFI) technique for detecting only the higher Rydberg states supplied from the lower Rydberg states due to the energy exchange. In this technique, the first pulsed electric field (F_1) discriminates free kinetic electrons and very high-lying Rydberg electrons just below the ionization threshold generated by the optically pumping. Some time after (typically ~ 1 μs), the second pulsed electric field (F_2) ionizes high-lying Rydberg states and these electrons are detected as ZEKE-PFI signal. The ZEKE-PFI signal consists of only the Rydberg electrons in the detection window determined by the strength of F_2. Both the Rydberg molecules initially populated by the optically pumping and supplied by the energy exchange may be observed under the condition $F_1 < F_2$. However, only the Rydberg molecules supplied by the energy exchange should be observed under the condition $F_1 > F_2$, since any initially populated Rydberg molecules are swept out by the stronger F_1. ZEKE-PFI signals were observed even under the condition $F_1 > F_2$ for poliatomic molecules like benzene and its derivatives, while not for the NO molecule. This fact strongly suggests that the internal energies of an ionic core excite Rydberg states to the higher excited Rydberg states.

VIII-B-2 Cation Vibrational Spectra of Pyrimidine and Its van der Waals Complexes with Ar and N_2 by ZEKE Photoelectron Spectroscopy

Shin-ichiro SATO, Kenji OMIYA *(Cyuubu Medical Co.)* **and Katsumi KIMURA**

[*J. Electron Spectrosc.* submitted]

Cation vibrational spectra of pyrimidine as well as the pyrimidine-Ar, -Ar_2 and -N_2 van der Waals (vdW) complexes have been obtained by means of ZEKE (zero kinetic energy) photoelectron spectroscopy for the first time. Four totally symmetric fundamental vibrations (ν_1, ν_{6a}, ν_{9a}, ν_{12}) and one non-totally symmetric vibration (ν_{6b}) of the pyrimidine cation have been assigned by using the respective five S1 vibrational levels as intermediate resonant states. *Ab initio* calculations (UHF/6-31G*, MP2/6-31G*, CASSCF/6-31G* and B3LYP/6-31G*) were also carried out for the vibrational frequencies of the pyrimidine cation to compare with the experimental values. The calculated frequencies of the 16*b* and 6*b* modes obtained from the UHF and CASSCF calculations are deviated from the experimental ones, but in good agreement with the experimental values in the B3LYP calculations under C_{2v} symmetry. Four additional vibrational levels (ν_{8a}, ν_{16a}, ν_{16b}, ν_{19a}) found from the ZEKE spectra have been assigned on the basis of the calculated frequencies. The I_a values of the complexes were found to be lowered from the I_a value of bare pyrimidine (I_a = 75 261 ± 6 cm^{-1}) by 261 cm^{-1} for the Ar complex, by 516 cm^{-1} for the Ar_2 complex, and by 95 cm^{-1} for the N_2 complex. In the ZEKE spectrum of pyrimidine-Ar, three low-frequency vibrational modes (b_x, b_y, s_z) were also observed at 36, 40, and 50 cm^{-1}, respectively. The change in structure along with the $D_0 \rightarrow S_1$ transitions was estimated from the Franck-Condon analysis of the relative band intensities for the pyrimidine-Ar complex. Some results obtained from the MP2/3-21+G** ab initio calculations were also presented for the pyrimidine-Ar complex.

VIII-C Developments and Researches of New Laser Materials

Although development of lasers is remarkable, there are no lasers which lase in ultraviolet and far infrared regions. However, it is expected that these kinds of lasers break out a great revolution in not only the molecular science but also in the industrial world.

In this project we research characters of new materials for ultraviolet and far infrared lasers, and develop new lasers by using these laser materials.

VIII-C-1 Spectrum Control of Intense THz-Radiation from InAs under Magnetic Field Irradiated with Stretched Femtosecond Laser Pulses

Shinji IZUMIDA, Shingo ONO, Hideyuki OHTAKE, Zhenlin LIU and Nobuhiko SARUKURA

We have reported the significant enhancement of THz-radiation power from InAs under magnetic field irradiated with femtosecond optical pulses. The THz-radiation power exhibits almost quadratic dependence on the excitation power and higher magnetic field. Furthermore, the radiation spectrum is found to be controlled by the excitation pulsewidth. For the control of the spectrum of this intense THz radiation, we introduced a high dispersion prism pair to stretch the pulse duration. The pulse duration was changed from 260 to 1100 fsec (FWHM) in auto correlation. With this stretched pulse for the excitation, we can control center frequency of THz radiation as shown in Figure 1. The longer excitation pulse width resulted in lower center frequency.

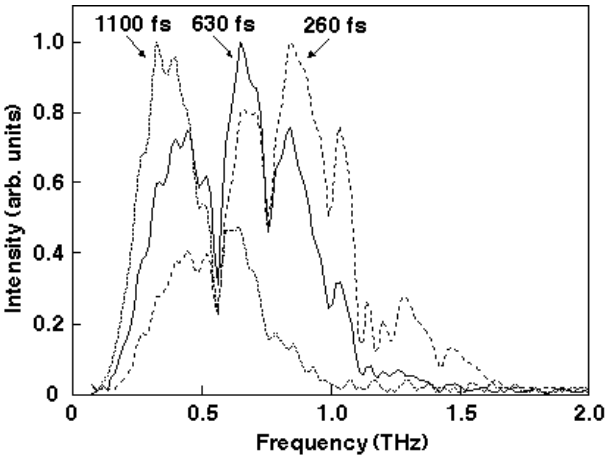

Figure 1. Spectrum of THz radiation excited with different pulse duration.

VIII-C-2 Estimation the Focusability of the THz Radiation

Shingo ONO, Shinji IZUMIDA, Zhenlin LIU, Takayuki YANO, Hideyuki OHTAKE, and Nobuhiko SARUKURA

We estimated the focusability of the THz radiation by measuring the intensity distribution of THz radiation. We can visualize the beam profile of THz-radiation propagation by using knife edge method as shown in Figure 1. THz radiation from the light source is collimated, focused, collimated, and focused onto a bolometer by four 10-cm off-axis parabolic mirrors. We measured in vertical and horizontal direction around the first focusing point using knife edge on the automatic translation stages. Figure 1 shows horizontal intensity distribution around the beam waist. The spot size at the beam waist reached about 1.5 mm. From this measurement, we propose that this spot size is good enough to perform pump and probe experiment in far infrared region.

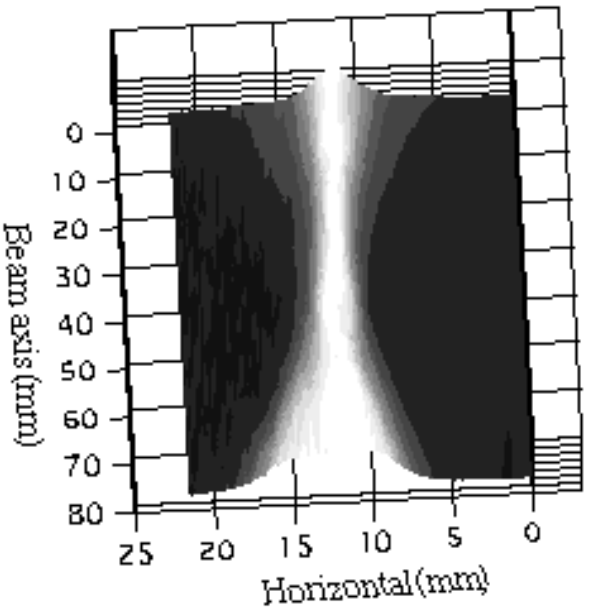

Figure 1. Horizontal intensity distribution of THz-radiation power around the beam waist.

VIII-C-3 Efficient, High Output Energy, Ultraviolet Ce:LiCAF Laser

Zhenlin LIU, Hideyuki OHTAKE, Nobuhiko SARUKURA, Kiyoshi SHIMAMURA *(Inst. Materials Research Tohoku Univ.)***, Na MUJILATU** *(Inst. Materials Research Tohoku Univ.)* **and Tsuguo FUKUDA** *(Inst. Materials Research Tohoku Univ.)*

The Ce^{3+}:$LiCaAlF_6$ (Ce:LiCAF) lasers have emerged as convenient, compact sources of tunable ultraviolet (UV) radiation in the spectral region from 281 to 315 nm. A UV solid-state Ce:LiCAF laser laser resonator is established by a flat high reflector and a flat output coupler with 30% reflection separated by 4 cm. The large Ce:LiCAF crystal (aperture 10 mm → 10 mm) which is doped with 1.2 mol% Ce^{3+} ions is located midway between the two cavity end mirrors. The fourth harmonic of a Q-switched Nd:YAG laser is used as the pumping source. The pump beam is focused with a 40-cm focal length lens to produce a spot size of φ4 mm at the surface of the Ce:LiCAF crystal. More than 85% of the incident pump energy was absorbed by the crystal. Figure 1 presents the obtained output energies at 290 nm as a function of the absorbed 266 nm pump energy. The laser oscillation threshold is 12 mJ, corresponds to a threshold fluence of approximately 100 mJ/cm^2. The measured output energy remained linear with pump fluence with an extremely good slope efficiency of 39%. The pulse energy as high as 21 mJ at 10 Hz at 290 nm, is the highest output energy reported from a Ce:LiCAF oscillator until now, to our knowledge.

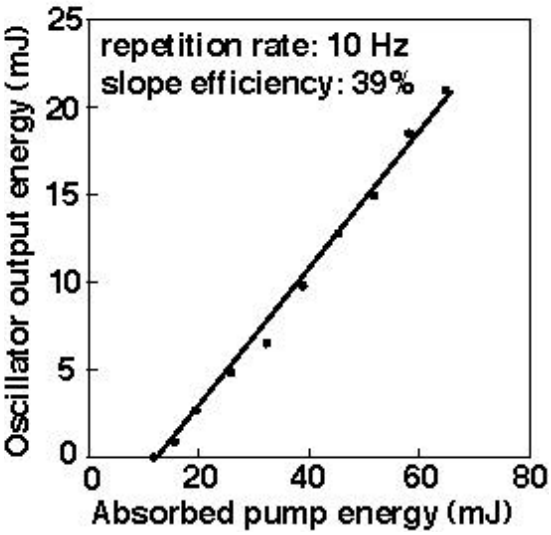

Figure 1. Laser output energy as a function of absorbed pump energy

VIII-C-4 All-Solid-State Tunable Ultraviolet Picosecond Ce^{3+}:$LuLiF_4$ Laser Pumped by the Fifth Harmonic of an Nd:YAG Laser

Zhenlin LIU, Hideyuki OHTAKE, Nobuhiko SARUKURA, Mark A. DUBINSKII *(Science & Engineering Services, Inc, USA)***, Ravil Yu. ABDULSABIROV** *(Kazan State Univ., Russia)* **and Stella L. KORABLEVA** *(Kazan State Univ., Russia)*

Due to the recent development of the fifth harmonic generation of Nd:YAG lasers, it becomes practical for the recently developed tunable solid-state UV laser material Ce^{3+}:$LiLuF_4$ (Ce:LLF) with tunability of about 305-340 nm to be directly pumped by the fifth harmonic of Nd:YAG lasers. Our optical layout for the short-cavity Ce:LLF laser is shown schematically in Figure 1. The Ce:LLF crystal with 0.2 at.% doping level was cut to form a cylinder ($\varphi 5 \rightarrow 25$ mm) with a flat polished window on the side. To geometrically reduce effective pumping penetration depth, the tilted-incidence-angle transverse pumping was used. To test the Ce:LLF laser tunability, a high-Q cavity was employed. The laser consisted of a dispersive Littrow-mounted 30°-prism with high reflection coated cathetus face and a low transmission flat output coupler (T = 20%). The 213-nm, 25-mJ, 5-nsec, horizontally polarized pulses (for σ-pumping) were stably obtained using the $(\omega + 4\omega)$ sum frequency generation process in $Li_2B_4O_7$ crystal. The Ce:LLF laser tunability obtained at the pumping energy of 22 mJ is from 309.5 nm to 312.3 nm and from 324.5 nm to 327.7 nm. For obtaining short pulses, a low-Q, short-cavity (6 cm) Ce:LLF laser was realized by replacing the above output coupler for an 80% transmission flat mirror. Using 16-mJ pumping pulses at 10-Hz repetition rate, we obtained 880-psec, 77-μJ, σ-polarized, and satellite-free pulses at 309-nm.

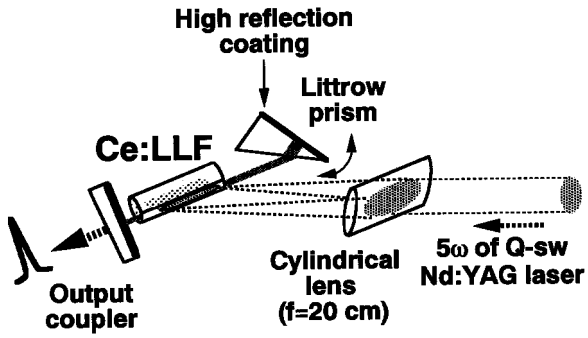

Figure 1. Short-cavity, tilted-incidence-angle ($\theta = 70°$) transverse pumping tunable Ce:LLF laser.

VIII-C-5 Broad-Band Gain Demonstration of New Yb:Glass

Zhenlin LIU, Hideyuki OHTAKE, Nobuhiko SARUKURA, Akihiko NISHIMURA *(Japan Atomic Energy Research Institute—Kansai Research Establishment)* **and Hiroshi TAKUMA** *(Japan Atomic Energy Research Institute—Kansai Research Establishment)*

Ytterbium:glass materials are interesting because they have long fluorescence lifetime, high saturation fluence and broad fluorescence band width. These characteristics make them particularly attractive for the generation of high peak power ultrashort pulses. A high power Yb:glass regenerative amplification has been demonstrated with the Chirped Pulse Amplification technique. The absorption and emission spectra of Yb:glass are much smoother than those of Yb:YAG. The broad gain of the Yb:glass was demonstrated through a pump-probe experiment. The pumping source was a dye (LDS925) laser pumped by the second harmonic of Q-SW Nd:YAG laser. It gave the pulse energy of 22 mJ at the wavelength of 930 nm. The probe beam came from a mode-locking Ti:sapphire laser (Tsunami, Spectra-Physics) pumped by an all solid-state green laser (Millennia X, Spectra-Physics). The 10 ps probe pulses are tunable ranging from 980 nm to 1065 nm. The pump and probe beams were overlapped colinearly through a dichroic mirror and then focused on to the Yb:glass (beam sizes: probe less than 300 μm/dia.; pump ~ 1 mm/dia.). The gain spectrum of the Yb:glass is shown in Figure 1. The gain spectrum of a Yb:YAG crystal is also shown in Figure 1 for comparison. The broad gain width of the Yb:glass has been confirmed with sufficient gain factors.

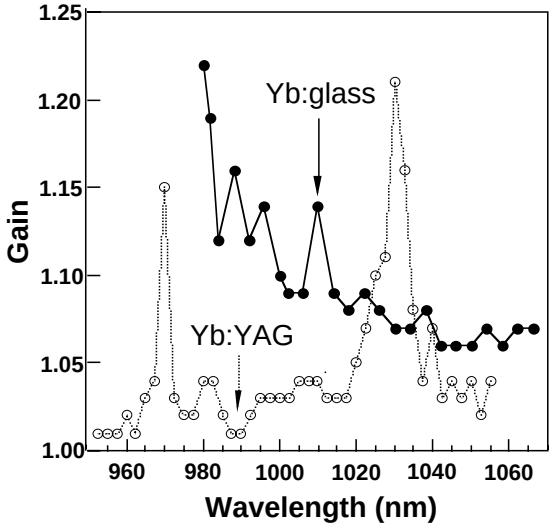

Figure 1. Gain spectrum of Yb:glass

VIII-C-6 Strong Enhancement of THz-Radiation Power from Femtosecond-Laser Irradiated InAs Clean Surface and Its Temperature Dependence

Hideyuki OHTAKE, Shingo ONO *(Science Univ. of Tokyo)***, Shinji IZUMIDA, Zhenlin LIU, and Nobuhiko SARUKURA, Kazuya WATANABE and Yoshiyasu MATSUMOTO**

We found strong enhancement of THz-radiation power from InAs (100) clean surface irradiated with femtosecond optical pulses. The clean surface was produced by Ar ion spattering method and we obtained clear LEED pattern after cleaning and 30 minutes annealing. The THz-radiation power became about three times larger than before cleaning. We have also found that THz-radiation power has strong temperature dependence. As shown in Figure 1, the power of THz-radiation at 50 K reaches about one order of magnitude higher than that at 450 K. Since we did not observe any changes of THz-radiation spectral shape, the origin of this radiation is the same at any temperature. This strong temperature dependence of THz-radiation power might be due to temperature dependence of carrier density.

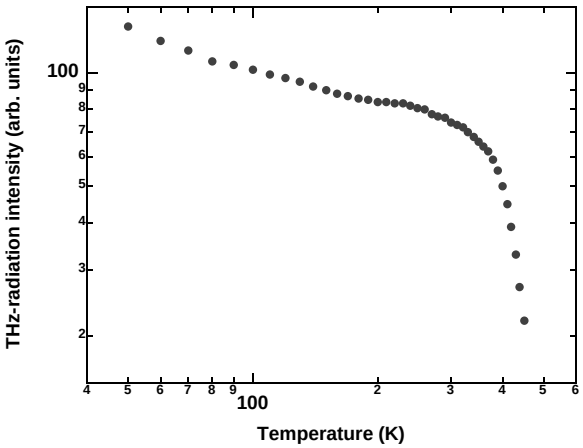

Figure 1. Temperature dependence of THz-radiation power. THz radiation from InAs (100) increases dramatically as temperature decreases.

VIII-D Development and Research of Advanced Tunable Solid State Laser Sources

The use of diode lasers to pump solid-state lasers leads to favorable performance characteristics. Diode-pumped solid-state lasers are compact, long-lived, and efficient sources of coherent radiation. They can provide excellent spatial mode quality and narrow linewidths. Because of the improved beam quality of diode-pumped solid-state lasers, nonlinear frequency conversion can readily be applied. Moreover, the availability of new and improved nonlinear optical crystals makes these techniques more practical. These kind advanced tunable solid-state light sources will assist the research of molecular science.

In this projects we research new Diode-Pumped Solid-State Lasers and new frequency conversion devices.

VIII-D-1 Intracavity Frequency Doubled Yb:YAG Miniature Laser

Takunori TAIRA, Jiro SAIKAWA, Eiji YAMAGUCHI *(Fukui Univ.)***, Takao KOBAYASHI** *(Fukui Univ.)* **and Robert. L. BYER** *(Stanford Univ.)*

Compact and efficient visible source of stable, single-frequency radiation are of potential interest for many applications such as display, interferometer and holographic systems. However, current argon-ion lasers suffer from low efficiency, short lifetimes and low coherency. Alternatively, as green lasers such as frequency doubled Nd-doped lasers are poor tunability and far from 515 nm.

In other hand, diode-pumped Yb:YAG laser which is promising material as a high power and high efficiency laser also have a potential for a wide tunable and high power mode lock lasers.[1-3] We also have reported a cw single-frequency and wide tunable Yb:YAG miniature laser.[4] Subsequently, frequency doubled Yb:YAG laser is one alternative technique to obtain single-frequency tunable light source around 515 nm region. We report our recent results for tunable single axial-mode oscillation of intracavity frequency doubled Yb:YAG miniature lasers.

The experimental configuration of the laser is shown in Figure 1. A maximum output power in single axial mode of 150 mW cw was achieved at 516nm with stability of ±1.7% during 15 minute. For frequency tuning, an intracavity birefringent filter was used. We obtained 10.9 nm(12.4THz) tunability around 516 nm by using 2-mm KTP crystal.

References
1)H. W. Bruesselbach, *et al*., *IEEE JSTQE.* **3**, 105 (1997).
2)A. Giesen, *et al.*, *OSA TOPS on Advanced Solid-State Lasers.* **10**, 280 (1997).
3)C. Honninger, *et al.*, *Opt. Lett.* **20**, 2402 (1995).
4)T. Taira, *et al*., *IEEE JSTQE.* **3**, 100 (1997).

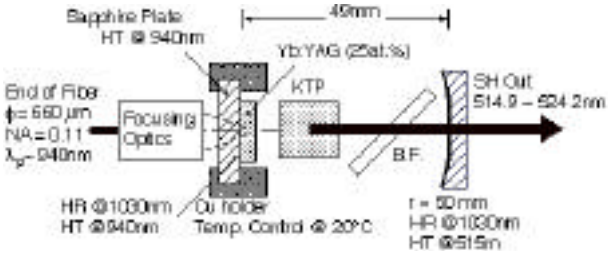

Figure 1. Schematic of the Intracavity frequency doubled Yb:YAG laser.

VIII-D-2 Design of Longitudinally Solid-State Lasers by Using M^2 Pump-Beam Factor

Takunori TAIRA, Nicolaie PAVEL *(Inst. Atm. Phy., ROMANIA)***, Mitsuyoshi FURUHATA** *(Fukui Univ.)***, Masato OHTAKA** *(Fukui Univ.)***, Takao KOBAYASHI** *(Fukui Univ.)* **and Hiromasa ITO** *(Tohoku Univ.)*

A model for optimization of longitudinally pumped solid-state lasers, in which the pump-beam was described by its M^2 factor, is proposed. Using the mode-overlap integrals, numerical investigations were carried out to obtain the optimum focusing position and pump beam waist, that ensure a minimum threshold pump power and maximum overlap efficiency, at a defined laser beam spot-size. The numerical data were fitted with analytical functions of pump beam M^2 factor, active medium absorption coefficient at the pump wavelength and laser beam volume. The experiments were performed with a Nd:YAG laser, longitudinally pumped with a maximum 10W fiber-coupled diode laser system and a Nd:YVO_4 miniature laser, pumped by a max. 1W array diode laser. Figure 1 shows Output power as a function of pump power for the Nd:YVO_4 laser. A fairly good agreement with theory was obtained.

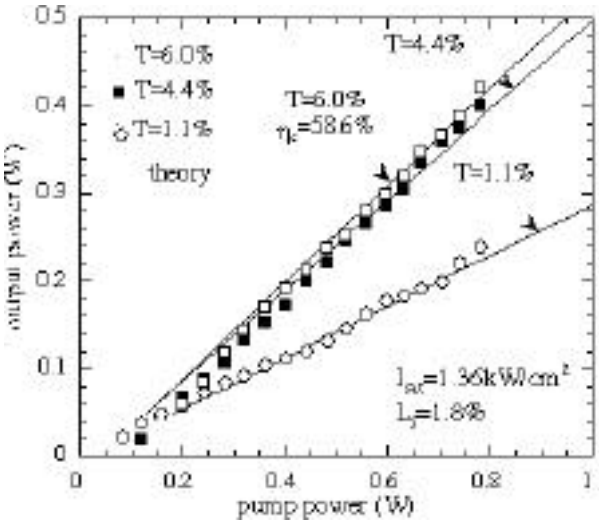

Figure 1. Output power as a function of pump power for the miniature Nd:YVO_4 system.

VIII-D-3 Diode-Pumped Nd:YAG Ceramics Lasers

Takunori TAIRA, Akio IKESUE *(Kurosaki Corp.)* **and Kunio YOSHIDA** *(Osaka Inst. Tech.)*

With the development of diode-pumped solid-state lasers during last decade, numerous laser materials have been developed and improved to achieve high efficiency and high power output. Nd:YVO_4 is in used as high efficiency miniature lasers because of its high absorption and emission cross-sections compare with Nd:YAG single crystal. However, its poor thermo-mechanical problems prevent high power operation. Much effort has gone into laser material research to find a high absorption coefficient laser medium with high thermal shock parameters.

Recently, we have developed a Nd:YAG ceramics with high optical quality.[1)] The YAG ceramics allows high neodymium-ion doping to overcome low absorption cross-section. Figure 1 shows the thermal conductivity of ceramics as a function of Nd concentration at 20°C. The YAG ceramic allows high neodymium-ion doping equal to high absorption and has high thermal conductivity compare with YAG single crystal and YVO_4. Therefore, Nd:YAG ceramics is promising new laser material for high efficiency and high power lasers.

We demonstrated, for the first time, a single-longitudinal-mode oscillation with ~ 213 mW output power, 17.6% slope efficiency using a Nd:YAG ceramics chip (4.8 at%). The threshold pump power was ~ 355 mW. For a 9.1 at% doped sample an effective absorption coefficien of 32.6 cm^{-1} was measured.

Reference
1) A. Ikesue, *et al.*, *J. Am. Ceram. Soc.* 78. 1033. (1995)

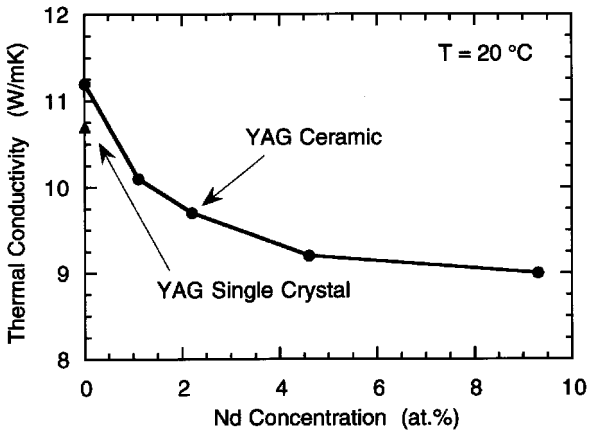

Figure 1. Thermal conductivity of the YAG ceramics as a function of Nd concentration.

Research Center for Molecular Materials

VIII-E Development of Novel Heterocyclic Compounds for Advanced Materials

Heterocycles containing chalcogen atoms are useful as components of organic conductors since heteroatoms in their rings are helpful to stabilize ions or ion-radical species, and extended π-conjugation decreases Coulombic repulsion. In addition intermolecular interactions caused by heteroatom contacts can be expected to form unique molecular assemblies. In this project novel electron acceptors, donors, and donor-acceptor compounds based on heterocycles such as 1,2,5-thiadiazole and 1,3-dithiole were synthesized and their properties including those of the charge-transfer complexes or ion-radical salts were investigated. Thiophene oligomers with rigid structures were also synthesized for molecular wires.

VIII-E-1 Synthesis and Characterization of New Electron Donors Containing 1,2,5-Thiadiazole and 1,1'-Dihydro-4,4'-bi(pyridylidene) Units

Yoshiro YAMASHITA, Katsuhiko ONO, Masaaki TOMURA and Kenichi IMAEDA

[*Chem. Commun.* 1851 (1997)]

Viologens **1** are widely used as electron-transfer reagents. However, their cation radical and neutral states are unstable toward oxygen due to their very low oxidation potentials. We have now introduced 1,2,5-thiadiazole rings to the dihydrobipyridine skeleton to give **2** in order to enhance the stability of the neutral state of viologens. The viologen derivatives **2** were prepared by reductive coupling of pyridinium compounds **3** which were obtained from 7-chloro-1,2,5-thiadiazolo[3,4-b]pyridine via several steps. The compounds **2a**,**b** are stable in air, in contrast to the unstable neutral viologens. They have absorption maxima in the long wavelength region [**2a**: 623, **2b**: 627 nm in CH_2Cl_2]. The oxidation potentials are lower than those of TTF, indicating that they are stronger electron donors than TTF. The donor **2a** gave PF_6 and AsF_6 salts of the cation radical upon electrochemical oxidation. They are 1:1 salts and show semiconducting behaviour. X-ray structure analysis of the PF_6 salt revealed that the planar donor molecules are stacked in an interesting mode where one donor molecule bridges two other molecules. Another interesting feature is that a tape-like network of the donor molecules is formed by short S···N contacts (3.05 Å).

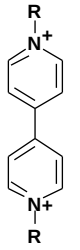

1

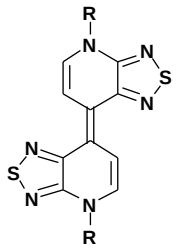

2a R = Me
2b R = Et

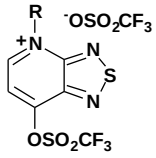

3

VIII-E-2 Synthesis and Properties of Bis(1,3-dithiol-2-ylidene) Compounds Containing a 2,2'-Bithienyl Unit

Akira OHTA and Yoshiro YAMASHITA

In order to develop new redox systems which undergo a reversible structural change by electron transfer, bis(1,3-dithiol-2-ylidene) compounds **1** containing a 2,2-bithienyl unit have been prepared by a Wittig-Horner reaction from the corresponding ketone. The cyclic voltammogram of **1a** shows an irreversible peak (E_{pa} = 0.82 V, E_{pc} = 0.28 V vs. SCE in PhCN). This result can be explained by considering that it undergoes an intramolecular oxidative cyclization and the resulting dication **2** reverts to **1** by reduction. In fact, chemical oxidation of **1a** with nitrosyl tetrafluoroborate afforded the corresponding cyclization products **2a** as a dication salt in 96% yield. The starting compound **1a** was reproduced by reduction of the dication salt with zinc dust in acetonitrile.

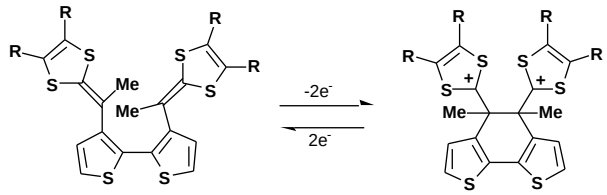

1 **a**: R, R = benzo **b**: R = SMe **2**

VIII-E-3 Synthesis and Properties of Novel Tetrathiafulvalene Vinylogues

Yoshiro YAMASHITA, Masaaki TOMURA, M. Badruz ZAMAN and Kenichi IMAEDA

[*Chem. Commun.* in press]

TTF vinylogues **1** bearing substituents at the vinyl positions have been considered to be non-planar due to the steric interactions between the substituents and the 1,3-dithiole parts. However, the TTF vinylogue skeletons can be planar when the aryl substituents are twisted from the π-conjugated framework. These compounds are expected to afford conductors with unusual structures since the bulky substituents disturb usual molecular overlapping. We have now synthesized

various derivatives **1** using an oxidative dimerization reaction of 1,4-dithiafulvene derivatives **2** with tris(4-bromophenyl)aminium hexachloroantimonate. The methyl, phenyl, and *p*- or *m*-substituted phenyl derivatives show reversible one-stage two-electron redox waves in their cyclic voltammograms, indicating that they are non-planar molecules and their cation radicals are unstable. In contrast, the derivatives with *o*-substituted phenyl groups show stepwise reversible oxidation potentials. This result suggests that the aryl part is twisted and the TTF vinylogue skeleton is planar in the cation radical states of the *o*-substituted phenyl derivatives. Actually, some compounds afforded the cation radical salts as single crystals upon electrochemical oxidation.

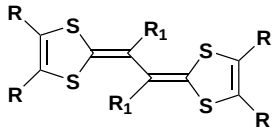

1

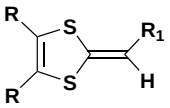

2

R, R = benzo, SCH_2CH_2S

VIII-E-4 Molecular and Crystal Structure of Novel Tetrathiafulvalene Vinylogues and Their Cation Radical Salts

Masaaki TOMURA and Yoshiro YAMASHITA

Molecular and crystal structures of novel tetrathiafulvalene (TTF) vinylogues and their cation radical salts with extended π-conjugated system and various functional groups in their vinyl part have been investigated by X-ray crystallographic analysis. In the compound **1a**, two 1,3-dithiole parts were twisted remarkably (dihedral angle: 61.1°). In contrast with the neutral state, the TTF vinylogue framework in the cation radical salt **1a**-PF_6 obtained by electrochemical oxidation was planar. Such a molecular structure causes an interesting two-dimensional stacking mode where one donor molecule bridges two molecules in the crystal of **1a**-PF_6, as shown in Figure 1. On the other hand, unique mixed stack was observed in the crystal of **1b**-$Au(CN)_2$ salt.

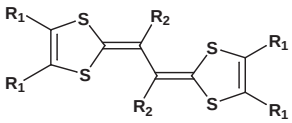

1

a: R_1,R_1 = benzo, R_2 = 2,6-$F_2C_6H_3$
b: R_1,R_1 = SCH_2CH_2S, R_2 = *o*-ClC_6H_4

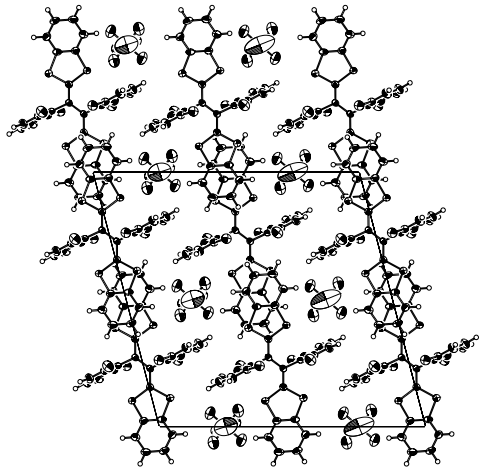

Figure 1. Crystal structure of **1a**-PF_6 salt viewed along b axis.

VIII-E-5 New Electron Acceptors Containing Thieno[3,4-b]pyrazine Units

Kazuharu SUZUKI, Masaaki TOMURA and Yoshiro YAMASHITA

[*J. Mater. Chem.* **8**, 1117 (1998)]

Sulfur containing TCNQ analogues are highly polarized and are expected to have strong intermolecular interactions by heteroatom contacts. Benzothiophene-TCNQ **1** is a weak electron acceptor due to the fused benzene ring. We have now replaced the benzene ring by electron-withdrawing pyrazine rings to give new acceptors **2**. We have also obtained π-extended acceptors **3** here. The acceptors **2** and **3** were prepared from 5,7-dibromothieno[3,4-b]pyrazines **4**. Thus, reaction of **4** with tetracyanoethylene oxide (TCNEO) in refluxing 1,2-dibromoethane afforded **2** and **3**. The cyclic voltammograms of **2** and **3** show reversible two-step one-electron redox waves. The reduction potentials are lower than those of TCNQ. The differences between the first and second reduction potentials are much lower in **3** than in **2** due to reduced on-site Coulomb repulsion. The single crystals of **2a** were obtained as two crystal forms, i.e. orthorhombic and monoclinic forms. In the orthorhombic crystal no short interheteroatom contact was observed. On the other hand, in the monoclinic crystal three kinds of short S···N contacts were observed, which result in an interesting helical structure. The acceptor **2a** gave two kinds of CT complexes with TTF (1:2 and 3:2 complexes) which have unique three-dimensional structures involving short S···N contacts.

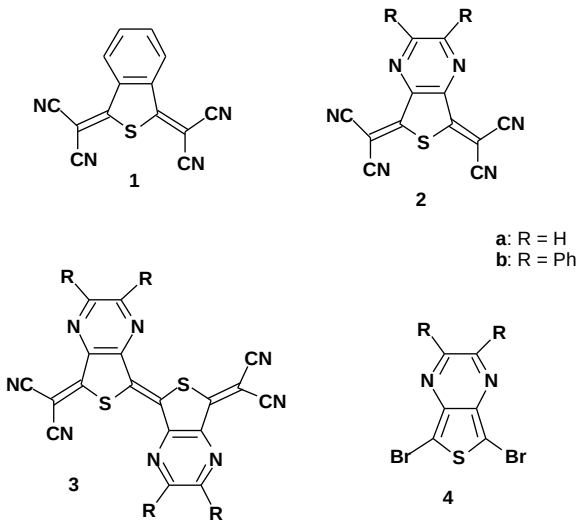

VIII-E-6 Design of Novel 4-Terminal Molecular Switching Unit Based on Multi-Stage Redox System

Shoji TANAKA and Yoshiro YAMASHITA

There has been a great deal of interest in utilizing π-conjugated organic molecules for nano-scale electronic devices. The main issue of molecular design in this area is to realize steady-state single-molecule conduction and quick switching of the conductivity (switching frequency > 1 T Hz). For this purpose, intensive efforts are now in place to synthesize transistor-like conjugated molecules with three or more distinct terminals, which would lead to dynamic control of information carries. As a novel building unit for this class of functional molecules, we have designed a "4-terminal" conjugated heterocyclic compound **2**. This molecule contains a pyrazine-dihydropyrazine multi-stage redox center **1** and the electronic structure can be switchable between low and high energy-gap states by chemical or electrochemical methods.

Compound **2red** was synthesized from 3',4'-diamino-2,2':5',2''-terthiophene. The reaction of **2red** with nickel peroxide gave the oxidized form **2ox**. AM1 calculations indicate that the unsubstituted redox center **1** has a much lower HOMO-LUMO gap in the oxidized form compared with that in the reduced form. Further, conformational analyses predict that the oxidized form **2ox** has a fully-conjugated π-system with all *s-trans* coplanar conformation, while the reduced form **2red** has a non-planar geometry. These theoretical predictions are consistent with the spectral data; the longest λ_{max} of **2ox** (1062 nm) appears at a much longer wavelength than that of **2red** (360 nm). We are trying to develop synthetic approaches for selective introduction of various types of molecular wires to each terminal (unsubstituted α or β-positions of the thiophene rings) of **2** to construct a molecular-scale transistor.

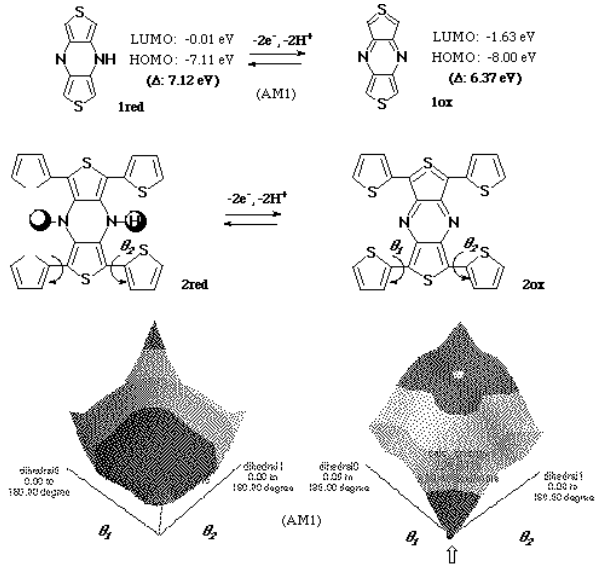

Figure 1. FMO levels of **1** and torsional potentials of **2** as a function of dihedral angles θ_1 and θ_2.

VIII-F Elecrtonic Structures and Rectivities of Active Sites of Metalloproteins

Metalloproteins are a class of biologically important macromolecules which have various functions such as oxygen transport, electron transfer, oxidation, and oxygenation. These diverse functions of metalloproteins have been thought to depend on the ligands from amino acid, coordination structures, and protein structures in immediate vicinity of metal ions. In this project, we are studying the relationship between the structures of the metal active sites and functions of metalloproteins.

VIII-F-1 Imidazole and *p*-Nitrophenolate Complexes of Oxo Iron(IV) Porphyrin π-Cation Radicals as Models for Compounds I of Peroxidase and Catalase

Hiroshi FUJII, Tetsuhiko YOSHIMURA *(Inst. for Life. Supp. Tech.)* **and Hitoshi KAMADA** *(Inst. for Life. Supp. Tech.)*

[*Inorg. Chem.* **36**, 6142 (1997)]

Oxo iron(IV) porphyrin π-cation radical species (compound I) have been identified or proposed as functional intermediates in the catalytic cycles of peroxidase, catalase, and cytochrome P-450. Since these enzymes have different axial ligands: peroxidase (imidazole), catalase (phenolate), and cytochrome P-450 (thiolate), the axial ligands are generally thought to control the reactivity of compounds I. To investigate the functional role of the axial ligand in compound I, we prepared and characterized imidazole, $(P^{\cdot})Fe^{IV}O(Im)$, and phenolate, $(P^{\cdot})Fe^{IV}O(OAr)$, complexes of oxo

iron(IV) 2,7,12,17-tetramethyl-3,8,13,18-tetramesityl porphyrin. $(P^{\cdot})Fe^{IV}O(Im)$ was prepared by titration of perchlorate oxo iron(IV) porphyrin π-cation complex, $(P^{\cdot})Fe^{IV}O(ClO_4)$, with one equivalent of imidazole. $(P^{\cdot})Fe^{IV}O(Im)$ was also formed when a mono imidazole complex of iron(III) porphyrin was oxidized by ozone in dichloromethane at -80°C. The successful formation of $(P^{\cdot})Fe^{IV}O(Im)$ can be attributed to the weak ligand character of the perchlorate anion which is easily displaced by imidazole and/or the use of ozone which does not form a coordinative ligand during the oxidation. The absorption spectrum of $(P^{\cdot})Fe^{IV}O(Im)$ closely resembled that of compound I in peroxidase. The paramagnetic ^{1}H-NMR of $(P^{\cdot})Fe^{IV}O(Im)$ indicates an a_{1u} radical state as well as imidazole coordination without reduction of the porphyrin π-radical. Similarly, a p-nitrophenolate complex of oxo iron(IV) porphyrin, $(P^{\cdot})Fe^{IV}O(OAr)$, was prepared by ozone oxidation of a mono *p*-nitrophenolate complex of iron(III) porphyrin in dichloromethane at -95°C. The absorption spectrum of $(P^{\cdot})Fe^{IV}O(OAr)$ closely resembled that of compound I of catalase. The results in this study indicate that the position of the absorption peak in compound I species correlates with the basicity of the axial ligand, but not the a_{1u}/a_{2u} porphyrin radical state.

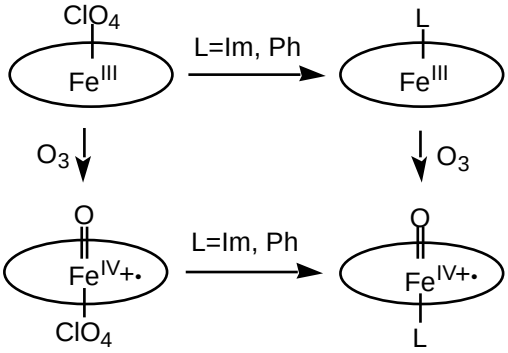

Figure 1. Synthesis of imidazole and *p*-nitrophenolate complexes of oxo iron(IV) porphyrin π-cation radicals.

VIII-F-2 Electron Configuration and Spin Distribution in Low-Spin (meso-Tetraalkylporphyrinato)iron(III) Complexes Carrying One or Two Orientationally Fixed Imidazole Ligands

Mikio NAKAMURA *(Toho Univ.)*, **Takahisa IKEUE** *(Toho Univ.)*, **Hiroshi FUJII, Tetsuhiko YOSHIMURA** *(Life for Supp. Tech.)* **and Kunihiko TAJIMA** *(Kyoto Inst. Tech.)*

[*Inorg. Chem.* **37**, 2405 (1998)]

To understand the orientation effect of coordinated imidazole ligands, a series of low-spin (tetraalkylporphyrinato)iron(III) complexes, $[Fe(TRP)(L)_2]^+$ and [Fe(TRP)(L)(CN)], carrying at least one orientationally fixed imidazole (L) have been prepared. The ^{1}H NMR pyrrole signals of a series of $[Fe(TRP)(2\text{-}MeIm)_2]^+$ have shown considerable downfield shifts as the meso substituent becomes bulkier, from -30.4 (R = H) to +5.6 ppm (R = iPr) at -71°C. The spread of the pyrrole signals decreases from 9.4 (Me) to 8.2 (Et) and then to 5.7 (iPr) ppm. The downfield pyrrole signals together with the small spread in $[Fe(TiPrP)(2\text{-}MeIm)_2]^+$ are in sharp contrast to the other low-spin complexes with orientationally fixed imidazole ligands; the chemical shifts and spreads of the pyrrole signals in [tetrakis-(2,4,6-trialkylphenyl)porphyrinato]iron(III) complexes $[Fe(R\text{-}TPP)(2\text{-}MeIm)_2]^+$ (R = Me, Et, iPr) are ca. -20 and ca. 9 ppm, respectively, at -71°C. The EPR spectra of a series of $[Fe(TRP)(2\text{-}MeIm)_2]^+$ were then taken at 4.2 K. While the R = H, Me, and Et complexes have shown so-called "large gmax type" spectra as in the case of $[Fe(R\text{-}TPP)(2\text{-}MeIm)_2]^+$, the iPr complex has exhibited an "axial type" spectrum. The result indicates that the electron configuration of the ferric ion of $[Fe(TiPrP)(2\text{-}MeIm)_2]^+$ is presented by the unusual $(dxz, dyz)^4(dxy)^1$ in contrast to the other low-spin complexes where ferric ions have the $(dxy)^2(dxz, dyz)^3$ configuration. When one of the 2-MeIm ligands in $[Fe(TRP)(2\text{-}MeIm)_2]^+$ is replaced by CN^-, not only the iPr but also the Me and Et complexes have shown the $(dxz, dyz)^4(dxy)^1$ configuration as revealed from the EPR spectra. The pyrrole signals of the iPr complex [Fe(TiPrP)(2-MeIm)(CN)] have been observed at 12.2, 14.1, 14.8, and 16.2 ppm at -71°C. Thus, the spread is only 4.0 ppm. The value is quite different from that of the corresponding [Fe(Me-TPP)(2-iPrIm)(CN)] where the spread reaches as much as 11.4 ppm. On the basis of these results, it is concluded that the spin distribution on the pyrrole -carbons in the complexes with $(dxz, dyz)^4(dxy)^1$ is rather homogeneous even if the coordinated imidazole is orientationally fixed. On the contrary, the fixation induces a larger asymmetric spin distribution on these carbons in the complexes with $(dxy)^2(dxz, dyz)^3$ configuration.

VIII-F-3 Raman Signature of the Fe_2O_2 "Diamond" Core

Elizabeth C. WILKINSON *(Univ. Minnesota)*, **Yanhong DONG** *(Univ. Minnesota)*, **Yan ZANG** *(Univ. Minnesota)*, **Hiroshi FUJII, Robert FRACZKIEWICZ** *(Univ. Houston)*, **Grazyna FRACZKIEWICZ** *(Univ. Houston)*, **Roman S. CZERNUSZEWICZ** *(Univ. Houston)* **and Lawrence QUE, JR.** *(Univ. Minnesota)*

[*J. Am. Chem. Soc.* **120**, 955, (1998)]

We report the resonance Raman (RR) spectra of iron complexes containing the $Fe_2(\text{-}O)_2$ core. Frozen CH_3-CN solutions of the FeIIIFeIV intermediate $[Fe_2(\text{-}O)_2\text{-}L_2](ClO_4)_3$ (where L = TPA, 5-Me_3-TPA, 5-Me_2-TPA, 5-MeTPA, 5-Et_3-TPA, or 3-Me_3-TPA) show numerous resonance-enhanced vibrations, and among these, an oxygen-isotope-sensitive vibration around 667 cm^{-1} that shifts ca. 30 cm^{-1} when the samples are allowed to exchange with $^{18}OH_2$, and whose Raman shift does not vary with methyl substitution of the TPA ligand. Spectra of iron-isotope-substituted samples of $[Fe_2(\text{-}O)_2(L)_2](ClO_4)_3$ (^{54}Fe and ^{57}Fe for L = TPA, and ^{54}Fe and ^{58}Fe for L = 5-Me_3-TPA) show that this vibration is also iron-isotope-sensitive. These isotopic data taken together strongly suggest that this vibration involves motion of the $Fe_2(\text{-}O)_2$ core that is isolated from motions of the ligand. A frozen CH_3CN solution of the

diiron(III) complex $[Fe_2(-O)_2(6\text{-}Me_3\text{-}TPA)_2](ClO_4)_2$ shows one intense resonance-enhanced vibration at 692 cm^{-1} that shifts -30 cm^{-1} with ^{18}O labeling. Normal coordinate analysis of the $Fe_2(-O)_2$ core in $[Fe_2(-O)_2(5\text{-}Me_3\text{-}TPA)_2](ClO_4)_3$ supports the assignment of the Fermi doublet centered around 666.2 cm^{-1} as an A_1 vibration of this core. Furthermore, we propose that this unique feature found in the region between 650 and 700 cm^{-1} is indicative of a diamond core structure and is the Raman signature of an iron cluster containing this core.

VIII-F-4 ^{63}Cu-NMR Study of Copper(I) Carbonyl Complexes with Various Hydrotris(pyrazolyl)-borates: Correlation between ^{63}Cu Chemical Shifts and CO Stretching Vibrations

Sadako IMAI *(Tokyo Inst. Tech.)*, **Kiyoshi FUJISAWA** *(Tokyo Inst. Tech.)*, **Takako KOBAYASHI** *(Tokyo Inst. Tech.)*, **Nobuhiko SHIRASAWA** *(Tokyo Inst. Tech.)*, **Hiroshi FUJII, Tetsuhiko YOSHIMURA** *(Inst for Life Supp. Tech.)*, **Nobumasa KITAJIMA** *(Tokyo Inst. Tech.)* **and Yoshihiko MORO-OKA** *(Tokyo Inst. Tech.)*

[*Inorg. Chem.* **37**, 3066 (1998)]

Copper(I) carbonyl complexes with a series of hindered LR_1,R_2 ligands (L: hydrotris(pyrazolyl)borate, R_1 and R_2 are substituents at the 3- and 5-positions of the pyrazole ring, respectively), LR_1,R_2CuCO [R_1, R_2 = Me, Me (1), i-Pr, i-Pr (2), t-Bu, Me (3), t-Bu, i-Pr (4), Ph, i-Pr (5), Ph, Ph (6)] have been synthesized and characterized by ^{1}H NMR and IR spectroscopy and elemental analysis. The molecular structures of 3 and 6 have been determined by X-ray crystallography. The electronic structures of copper(I) sites are characterized by means of ^{63}Cu NMR spectroscopy and by the CO stretching vibration. The sharp ^{63}Cu NMR signals are observed for LR_1,R_2CuCO complexes in toluene at room temperature. The ^{63}Cu NMR signals of copper(I) complexes with alkyl-substituted ligands (1-4) are observed in lower field than those of the phenyl derivatives (5, 6) correlating with the electron-density at the copper center. This argument is supported by the good correlation between the (^{63}Cu) value and CO stretching vibration which is a sensitive indicator of the extent of back-donation of the Cu d electrons to the antibonding CO orbitals.

VIII-G Molecular Mechanism of Heme Degradation and Oxygen Activation by Heme Oxygenase

Heme oxygenase (HO), an amphipathic microsomal proteins, catalyzes the regiospecific oxidative degradation of iron protoporphyrin IX (heme) to biliverdinIXα, carbon monoxide, and iron in the presence of NADPH-cytochrome P-450 reductase, which functions as an electron donor. Heme oxygenase reaction is the biosynthesis processes of bile pigments and CO which is a possible physiological messenger. Recent development in the bacterial expression of a soluble form of heme oxygenase has made it possible to prepare in the large quantities for structural studies. In this project, we are studying the molecular mechanism of heme degradation and oxygen activation by heme oxygenase using various spectroscopic methods.

VIII-G-1 Cobalt Porphyrin Heme Oxygenase Complex. EPR Evidences for the Distal Heme Pocket Hydrogen Bonding

Hiroshi FUJII, Yi DOU *(Case Western Reserve Univ.)*, **Hong ZHOU** *(Yamagata Univ.)*, **Tadashi YOSHIDA** *(Yamagata Univ.)* **and Masao IKEDA-SAITO** *(Case Western Reserve Univ.)*

[*J. Am. Chem. Soc.* **120**, 8251 (1998)]

Heme oxygenase (HO) is a microsomal enzyme which catalyzes the degradation of iron protoporphyrin IX (heme) to biliverdinIXα through the two heme derivatives, α-meso-hydroxyheme and verdohemeIXα. The key intermediate in the first step of the heme oxygenase reaction is the metastable ferrous O_2-bound form of the heme-HO complex. While our resonance Raman studies of the oxy-form indicated a highly bent structure of bound dioxygen, the electronic structure and the activation mechanism, including the proton relay system using hydrogen bond interaction with bound dioxygen, need to be elucidated. To this end, we have prepared the cobalt(II) porphyrin HO complex. The EPR spectrum of deoxy-form of the cobalt(II) porphyrin HO complex is similar to that of cobalt-myoglobin (Mb), indicating the similarity of the binding property of proximal histidine between them. In contrast, the EPR spectrum of the oxy-from of cobalt porphyrin HO complex is more anisotropic than that of cobalt-Mb. This reflects the difference in the structure of bound dioxygen between them. The EPR parameters seem to be consistent with the highly bent Co-dioxygen binding. When the measurement is carried out in a deuterated buffer system, the hyperfine structure of the EPR spectrum of the oxy form of the cobalt-HO complex is sharpened. This shows the formation of a hydrogen bond interaction between the bound dioxygen and the amino acid residue in the distal pocket of the enzyme. The finding of the hydrogen bond interaction could explain the high oxygen affinity of the heme-HO complex and the meso hydroxylation mechanism using proton relay system proposed for cytochrome P-450.

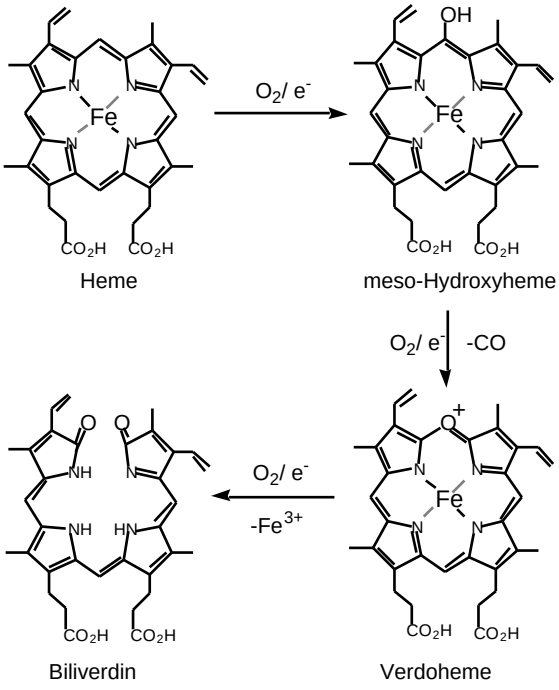

Figure 1. Reaction intermediates in the heme oxygenase-catalyzed oxidation of heme to biliverdinIXα.

VIII-G-2 The Oxygen and Carbon Monoxide Reactions of Heme Oxygenase

Catharina Taiko MIGITA *(Case Western Reserve Univ.)*, **Kathyln Mansfield MATERA** *(Case Western Reserve Univ.)*, **Masao IKEDA-SAITO** *(Case Western Reserve Univ.)*, **John S. OLSON** *(Rice Univ.)*, **Hiroshi FUJII, Hong ZHOU** *(Yamagata Univ.)* **and Tadashi YOSHIDA** *(Yamagata Univ.)*

[*J. Biol. Chem.* **273**, 945 (1998)]

Heme oxygenase is the central enzyme of heme degradation and associated carbon monoxide biosynthesis. We have prepared the heme, α-hydroxyheme, and verdoheme complexes of heme oxygenase, and their reactions with oxygen and carbon monoxide have been studied. The heme complexes of heme oxygenase isoforms-1 and -2 have similar oxygen and carbon monoxide binding properties. The oxygen affinities are very high, K_{O_2} = 30 - 80 μM^{-1}, which is 30 to 90-fold greater than those of mammalian myoglobins. The oxygen association rate constants are similar to those for myoglobins (k'_{O_2} = 7-20 $\mu M^{-1}s^{-1}$), whereas the oxygen dissociation rates are remarkably slow (k_{O_2} = 0.25 s^{-1}), implying the presence of very favorable electrostatic interactions between bound oxygen and protein residues in the heme pocket. The carbon monoxide association reactions with the heme-enzyme complexes are biphasic, while the CO dissociation reactions are monophasic. The carbon monoxide affinities estimated for both isoforms are only 1 to 6-fold higher than the corresponding oxygen affinities. Thus, both HO-1 and HO-2 discriminated much more strongly against CO binding than either myoglobin or hemoglobin. The carbon monoxide binding reactions with the ferrous a-hydroxyheme-HO complex are similar to those of the initial protoheme complex, and thus hydroxylation at the a-meso position does not appear to affect the reactivity of the iron atom. In contrast, the carbon monoxide affinities of the verdoheme-HO complexes are > 10,000 times weaker that those of the heme complexes due to a 100-fold slower association rate constant ($k'_{CO} \approx 0.004\ \mu M^{-1}$) and a 300-fold greater dissociation rate constant (kCO ≈ 3 s^{-1}) compared to the corresponding rate constants of the protoheme and a-OH heme complexes. The positive charge on the verdoporphyrin ring causes a large decrease in reactivity of the iron.

VIII-G-3 Identification that Histidine 45 is the Axial Heme Iron Ligand of Heme Oxygenase-2

Kazunobu ISHIKAWA *(Yamagata Univ.)*, **Kathyln Mansfield MATERA** *(Case Western Reserve Univ.)*, **Hong ZHOU** *(Yamagata Univ.)*, **Hiroshi FUJII, Michihiko SATO** *(Yamagata Univ.)*, **Tetsuhiko YOSHIMURA** *(Inst. for Life. Supp. Tech.)*, **Masao IKEDA-SAITO** *(Case Western Reserve Univ.)* **and Tadashi YOSHIDA** *(Yamagata Univ.)*

[*J. Biol. Chem.* **273**, 4317 (1998)]

A truncated, soluble, and enzymatically active form of human heme oxygenase-2(ΔHHO2) was expressed in *Escherchia coli*. To identify the axial heme ligand of HO-2, His-45 to Ala(ΔH45A) and His-152 to Ala (ΔH152A) mutants have been prepared using this expression system. ΔH45A could form a 1:1 complex with hemin but was completely devoid of the heme degradation acitivty. A 5-coordinate-type ferrous NO EPR spectrum was observed for the heme-ΔH45A complex. The ΔH152A mutant was expressed as an inclusion body and was recovered from the lysis pellet by dissolution in urea followed by dialysis. The solubilized fraction obtained, however, was composed of a mixture of a functional enzyme and an inactive fraction. The inactive fraction was removed by Sephadex G-75 column at the void volume. The gel filtration-purified ΔH152A exhibited spectroscopic and enzymatic properties identical to those of wild-type. We conclude, in contrast to the previous reports (McCoubrey and Mains, *Arch. Biochem. Biophys.* **302**, 402 (1993); McCoubrey, W. K., Jr., Huang, T. J. and Mains, M., *J. Biol. Chem.* **272**, 12568 (1997)), that His-45, but not H152, in heme oxygenase isoform-s is the proximal ligand of the heme and is essential for the heme degradation aciticty of the enzyme. His-152 appears to play a structural role in stabilization of the heme oxygenase protein.

VIII-H Designing Artificial Photosynthesis at Molecular Dimensions

Photosynthesis is one of the finest piece of molecular machinery that Nature has ever created. Its ultrafast electron transfer and following well-organized sequence of chemical transformation have been, and will continue to be, challenging goals for molecular scientists. We are trying to mimic the function of photosynthesis by assembling molecular units that perform individual physical/chemical action. The molecular units include porphyrins, redox active organic molecules, and transition metal complexes.

We have been so far focusing our efforts on manganese complexes (which are known to play a key role in oxygenic photosynthesis) and their interaction with porphyrins. Our ultimate goal is to design artificial molecular systems that effect multiple chemical reactions triggered by light, on the basis of molecular rationale.

VIII-H-1 Synthesis and Characterization of Manganese Complexes

Hitoshi IIKURA *(Kyoto Univ.)* **and Toshi NAGATA**

[*Inorg. Chem.* in press]

Four new manganese complexes of carboxylate-containing chelating ligands, L^1 and L^2 (L^1H = (bis(2-pyridylmethyl)amino)acetic acid, L^2H = 3-(bis(2-pyridylmethyl)amino)propionic acid), were synthesized and characterized by X-ray crystallography. In spite of the structural diversity in these complexes - two Mn^{II} dimers, one Mn^{II} chain complex, and one bis(μ-oxo) Mn^{IV} dimer - all of them were built up from a common structural motif, an "L^nMn" fragment, interconnected in various topology. These ligands L^1 and L^2 are potentially useful in controlling structures of manganese carboxylate complexes.

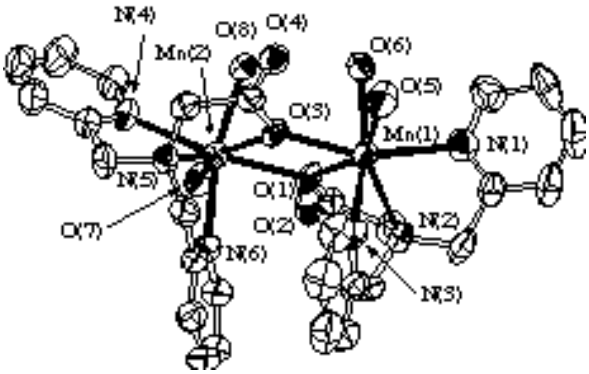

Figure 1. ORTEP view of the $[Mn_2L^1{}_2(H_2O)_4]^{2+}$ cation.

VIII-H-2 Synthesis and Photophysical Properties of Porphyrin-Dimanganese Composite Molecules

Katsuji AIKAWA *(Kyoto Univ.)***, Toshi NAGATA, Atsuhiro OSUKA** *(Kyoto Univ.)***, Yoshifumi KIMURA** *(Kyoto Univ.)***, Noboru HIROTA** *(Kyoto Univ.)***, Iwao YAMAZAKI** *(Hokkaido Univ.)* **and Yoshinobu NISHIMURA** *(Hokkaido Univ.)*

The first porphyrin-dimanganese composite molecules were synthesized. Fluorescence of the porphyrin moiety was effectively quenched by the dimanganese moiety (fluorescence lifetime decreased from 1.5 ns to 61 ps). Transient absorption spectoscopy revealed that intersystem crossing from S_1 of porphyrin to T_1 was enhanced by the presence of the manganese complex. Analogous compound with zinc in place of manganese did not show such enhancement, suggesting that the unpaired electrons on the manganese ions are involved in the process. Comparison of the electrochemical properties of the composite molecules with those of the component molecules (porphyrin and dimanganese complex), it was revealed that the oxidation potentials of dimanganese moieties showed about +0.1 V shift whereas the oxidation potentials of porphyrin showed no significant change.

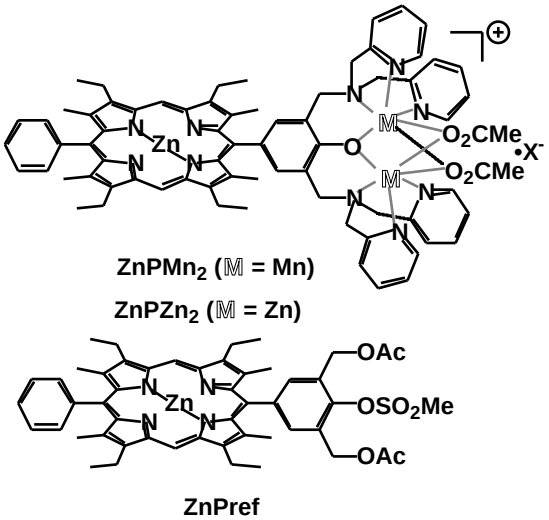

Figure 1. A porphyrin-dimanganese composite molecule and related compounds.

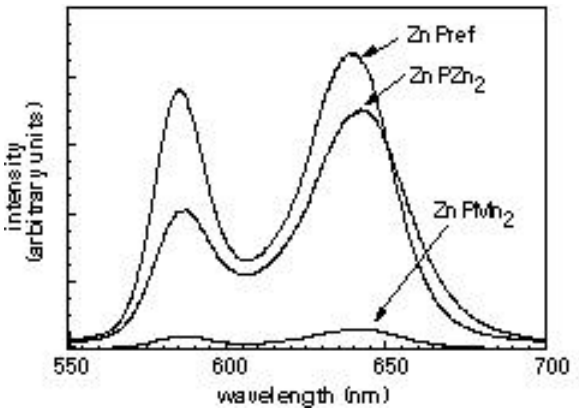

Figure 2. Steady-state fluorescence spectra (at room temperature, in CH_3CN).

VIII-I Organic Molecular Materials with Novel Electronic Properties

Some aromatic and heterocyclic compounds show intriguing physical properties, such as superconductivity, ferromagnetism, and electroluminescence, in the solid state. The aim of our research is to design and synthesize such molecules. We have been working on three research projects: synthesis of organic conductors, fullerene chemistry, and organic electroluminescent (EL) materials.

VIII-I-1 Functionalization of C_{60} by Acetylenes

Hiroshi YAMAGUCHI *(Nagoya Univ.)*, **Shizuaki MURATA** *(Nagoya Univ.)* **and Toshiyasu SUZUKI**

Unsaturated bonds in the organic groups on C_{60} are expected to interact with π orbitals of C_{60}, if the distance between these two π systems is close enough. Some of these examples are known to undergo unique intramolecular rearrangements. We are interested in constructing such C_{60} derivatives by using acetylenes.[1)] Thus, in the presence of Pd(0), two dimethyl acetylenedicarboxylate molecules react with C_{60} to give $(MeOCOC)_4C_{60}$. Under photochemical conditions, this derivative can be converted into the bis-methanofullerene isomer, which is easily oxidized to $(MeOCO)_4C_{60}O_2$ (Figure 1) with a large hole in the fullerene cage.

Reference

1)H. Yamaguchi, S. Murata, T. Akasaka and T. Suzuki, *Tetrahedron Lett.* **38**, 3529 (1997).

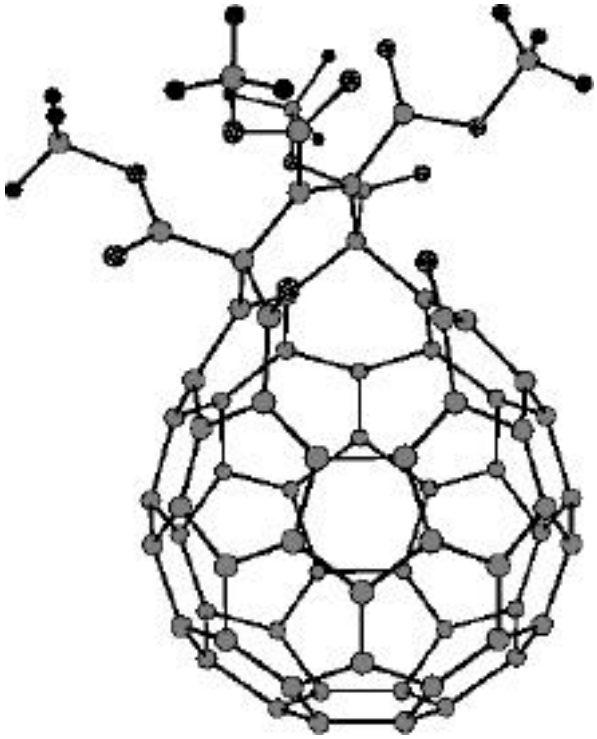

Figure 1. Molecular model of $(MeOCO)_4C_{60}O_2$.

VIII-I-2 New Electron-Transporting Materials for Organic EL Devices

Toshiyasu SUZUKI

Recently, organic EL devices have gained considerable attention because of their application to flat panel displays. These devices are composed of hole-transporting, emissive, and electron-transporting (ET) layers as well as two electrodes. Organic photoconductors (triaryl amine derivatives) and laser dyes can be adapted to hole-transporting and emissive materials, respectively. On the other hand, there have been few ET organic materials for practical use. We are trying to synthesize perfluorinated phenylene dendrimers which might form stable amorphous ET layers.

VIII-J Studies of Nanoscale Carbons

The sp^2 bonded nanometer scale carbons are studied in this project. Nanotubes and nano-graphite particles are the candidates of the materials. Electron microscopy, powder x-ray diffraction, Raman scattering, electron spin resonance and magnetic susceptibility measurements are all used to study the structural and solid state properties of nanoscale carbon materials.

VIII-J-1 Effect of Environment Temperature for Synthesizing the Single Wall Carbon Nanotubes by Arc Vaporization Method

Morio TAKIZAWA *(Japan Science & Technology Corporation)*, **Tatsuharu TORII and Shunji BANDOW** *(Japan Science & Technology Corporation)*

Single wall carbon nanotubes (SWNTs) can be synthesized either a pulsed laser vaporization at high temperature environment (~1200 °C) or an arc burning at room temperature of a carbon rod containing a few atomic % of bi-metallic catalysts such as Ni-Y, Ni-Co and Ni-Fe. The effect of the environment temperature for yielding SWNTs by the pulsed laser vaporization method has been reported previously.[1] Briefly, a synthesizing rate of SWNTs was accelerated at the temperature higher than 850 °C. In this study, we briefly report the effect of environment temperature to produce SWNTs via. the arc burning of a Ni-Y (0.6-0.6 atom %) catalyzed carbon rod. The arc burning of the carbon rod containing Ni-Y was carried out in a 50 mm diameter quartz tube under a 500 Torr of He gas. Environment temperature near the arcing was controlled by the electronic furnace surrounding the quartz tube. The number of SWNTs was estimated by measuring the diameter of tubule bundle D and by counting the number of bundles per unit area N. By using D^2N, we can estimate the number of individual tubules per unit area for each sample. Figure 1 shows the temperature effect for synthesizing the tubules. In Figure 1, we can find the SWNTs are well generated in the temperature range of 400 to 600 °C. According to the present study and to the laser vaporization study, it was found that the environment temperature is also important to synthesize SWNTs as well as to select the metal catalyst.

References

1) S. Bandow, S. Asaka, Y. Saito, A. M. Rao, L. Grigorian, E. Richter and P. C. Eklund, *Phys. Rev. Lett.* 80, 3779 (1998).

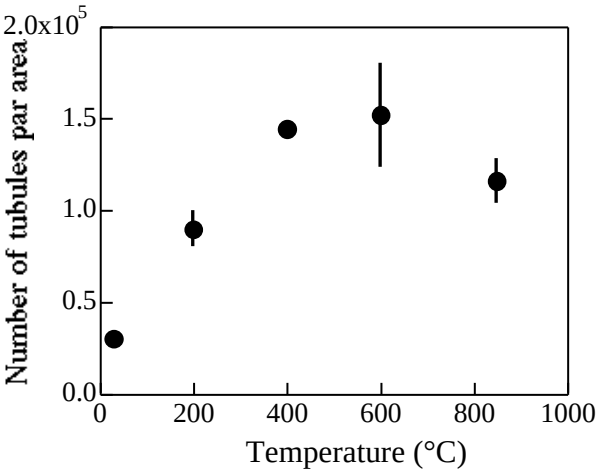

Figure 1. Environment temperature dependence on synthesizing the single wall carbon nanotubes via. arc burning of Ni-Y (0.6-0.6 atom %) composite carbon rod. The rod is 10 mm in diameter and is set at the end of the positive electrode. The arc current is 100 A under a 500 Torr of He gas with a flow rate of 100 sccm.

VIII-J-2 Radial Thermal Expansion of Purified Multiwall Carbon Nanotubes Measured by X-Ray Diffraction

Shunji BANDOW *(Japan Science & Technology Corporation)*

[*Jpn. J. Appl. Phys.* **36**, L1403 (1997)]

The thermal expansion in the radial direction (stacking axis of graphene sheets) of multiwall carbon nanotubes (MWNTs) is measured in the temperature range from 10 to 320 K. The sample includes in excess of 85 % by weight of MWNTs. The radial thermal expansion of MWNTs is found to be almost the same with the c-axis thermal expansion of graphite. This result strongly challenges the concentric structural model for MWNTs, suggesting the appropriateness of the scroll type model instead of the concentric one.

VIII-J-3 Effect of the Growth Temperature on the Diameter Distribution and Chirality of Single Wall Carbon Nanotubes

Shunji BANDOW *(Japan Science & Technology Corp.)*, **Shuji ASAKA, Yahachi SAITO** *(Mi'e Univ.)*, **Apparao M. RAO** *(Univ. Kentucky)*, **Leonid GRIGORIAN** *(Univ. Kentucky)*, **Ernest RICHTER** *(Univ. Kentucky)* **and Peter C. EKLUND** *(Univ. Kentucky)*

[*Phys. Rev. Lett.* **80**, 3779 (1998)]

Pulsed laser vaporization (PLV) of a heated, catalyzed carbon target in argon gas has been used to synthesize single-wall carbon nanotubes (SWNTs). Electron microscopy, x-ray diffraction and Raman spectroscopy were all used to study the effect of the catalyst on the tube yield, and the evolution of the tube diameter distribution with increasing growth environment temperature T. By controlling the temperature in the range $780 < T < 1050$ °C, we have been able to tune the diameter of the tubules from ~ 0.81 to ~ 1.51 nm. The threshold temperature for significant SWNT production was found to be ~ 850 °C.

VIII-J-4 Purification and Magnetic Properties of Carbon Nanotubes

Shunji BANDOW *(Japan Science & Technology Corp.)*, **Shuji ASAKA, X. ZHAO** *(Meijo Univ.)* **and Yoshinori ANDO** *(Meijo Univ.)*

[*Appl. Phys. A* **67**, 23 (1998)]

Purification procedures for both multi- (MWNTs) and single-wall carbon nanotubes (SWNTs) are introduced in this paper. Intermediate stages in the purification procedure are monitored by scanning electron microscopy, which clearly shows the increase of the nanotube content with increasing the purification. The magnetic properties are investigated by the electron spin resonance (ESR). Two kinds of samples are used in

the ESR measurements for MWNTs and for SWNTs. One is dispersed in hexane to make loosely contacting tubules, and the other is a dried-deposited tubules to realize a close contacting tubule state. By use of these samples, it is found that the ESR lineshape is closely related to the contact between nanotubes. The curved nature of the tube wall plays an important role to explain the ESR properties.

VIII-J-5 Raman Spectroscopy of Single Wall Carbon Nanotubes

Apparao M. RAO *(Univ. Kentucky)*, **Shunji BANDOW** *(Japan Science & Technology Corp.)*, **Ernest RICHTER** *(Univ. Kentucky)* **and Peter C. EKLUND** *(Univ. Kentucky)*

[*Thin Solid Films* in press]

Pulsed laser vaporization (PLV) of a heated, Fe/Ni or Co/Ni catalyzed carbon target in argon gas has been used to synthesize single-wall carbon nanotubes (SWNTs). The Raman spectrum of SWNTs is very different from that observed for graphite (the nanotube's flat parent) and these differences can be understood as a result of the cyclic boundary condition imposed on a graphene sheet rolled up to form a seamless nanotube. Optical resonances are observed which are associated with the one dimensional character of the electronic states of these novel quantum wires. The high frequency tangential mode frequency is significantly upshifted (downshifted) when the SWNT bundles are exposed to acceptor (donor) dopants.

VIII-J-6 The Structure and Electronic Properties of Graphite Nano-Particles

Odd E. ANDERSSON *(Tokyo Inst. Tech.)*, **B. L. V. PRASAD** *(Tokyo Inst. Tech.)*, **Hirohiko SATO** *(Tokyo Inst. Tech.)*, **Toshiaki ENOKI** *(Tokyo Inst. Tech.)*, **Yoshihiro HISHIYAMA** *(Musashi Inst. Tech.)*, **Yutaka KABURAGI** *(Musashi Inst. Tech.)*, **Masanori YOSHIKAWA** *(Tokyo Inst. Tech.)*, **Shunji BANDOW** *(Japan Science & Technology Corp.)*

[*Phys. Rev. B* submitted]

We have investigated the structure and electronic properties of graphite nano-particles prepared by heat-treating diamond nano-particles. The prepared nano-graphite forms a polyhedron with a hollow in its inside, whose faces comprise a stacking of 3-6 planar graphene sheets with the in-plane size of 7-8 nm and the inter-sheet distance of 0.353 nm. The large inter-sheet distance suggests a considerably large reduction in interlayer interaction compared to the case of bulk regular graphite. Electron spin resonance and magnetic susceptibility measurements show that there is a considerable enhancement in the density of states at the Fermi energy, indicating the presence of an additional band superimposed upon the bonding π and the antibonding π^* bands around the Fermi energy. Taking into consideration the discontinuous shape at an edge line formed by crossing adjacent graphene sheets, graphene sheets in a nano-graphite particle are considered to have open π-bond edges. On the basis of the theoretical suggestion that non-bonding π orbitals give edge-inherited surface states depending on the shape of the graphene edge, this is suggestive of the contribution of the novel edge states to the electronic structure of nano-sized graphene having open p-bond edges.

VIII-K The Measurement of Dipolar Interactions under Magic-Angle Sample Spinning

VIII-K-1 Dipolar Interactions between ^{13}C and ^{15}N

Daisuke KUWAHARA, Toshihito NAKAI *(Tsukuba Univ.)* **and Seiichi MIYAJIMA**

[*Chem. Phys. Lett.* **291**, 244 (1998)]

A novel and simple method for measuring heteronuclear dipolar spectra under magic-angle sample spinning is described; the present method utilizes a chemical-shift-anisotropy recovery technique exploited by Tycko, Dabbagh and Mirau in a two-dimensional NMR experimental scheme. ^{13}C-^{15}N dipolar powder spectrum was obtained to give a internuclear distance for a doubly labeled *L*-alanine. The present method will be extended to observe a heteronuclear dipolar interaction between ^{13}C and quadrupolar nuclei having integer spins such as ^{2}H or ^{14}N.

Equipment Development Center

VIII-L Development of "IMS Machines"

The technical staff of the Equipment Development Center is partly engaged in planning, researching, designing and constructing "IMS machines." This machine, crowned with the acronym of the Institute for Molecular Science, is a high-tech experimental instrument, with emphasis on new technical idea and co-operative work with members inside and outside the Institute including those in industries. We collect suggestions of new instruments once every year from all of the members of IMS.

In this fiscal year, 1997, three project themes (1 thorough 3) were adopted as IMS machines. IMS machine projects 3 and 4 (IMS machine 1996) below were completed.

1. **Surface Profiler of Mirrors for High-Resolution Monochromator**
   (proposed by Toyohiko KINOSHITA, developed with Hisashi YOSHIDA, Toshio HORIGOME, and Shuji ASAKA)
2. **Off-Axis Paraboloid Polarizing Mirror for Far-Infrared Light**
   (proposed and developed by Hideyuki OHTAKE and Takayuki YANO)
3. **Multi-Channel Detector for Mid-Infrared Light**
   (proposed by Takashi OGURA, developed with Hisashi YOSHIDA and Shuij ASAKA)
4. **Programmable Micro Current Source**
   (proposed and developed by Tomonori TOYODA)

Brief reports on the projects 3 and 4 are presented in the following.

VIII-L-1 Multi-Channel Detector for Mid-Infrared Light

Hisashi YOSHIDA, Shuji ASAKA and Takashi OGURA

We have developed a multi-channel detector for mid-infrared light by using a 256-channel MCT photoconductive array cell (HAMAMATSU, Figure 1). The block diagram of the present device is shown in Figure 2. The current signals from the MCT cells are amplified and integrated in respective 256 units of AC-coupled amplifier and gated integrators. The output from each integrator is fed to a computer channel by channel through a data multiplexer. There exists a difficulty in that the high gain amplifiers undergo large voltage drifts due to temperature change. We have overcome this point by adding a chopper in the incoming light source, gating the integrator to synchronize with the open and closed periods of the chopper, and finally taking the difference of the two integrated outputs. The subtraction is done in a software to reduce the loads to the hardware. Control and data processing are performed on a DOS machine, and this software was developed by use of VisualBasic. The appearance of the developed detector system is shown in Figure 3.

Figure 1. Outer view of 256-channel MCT photoconductive array cell.

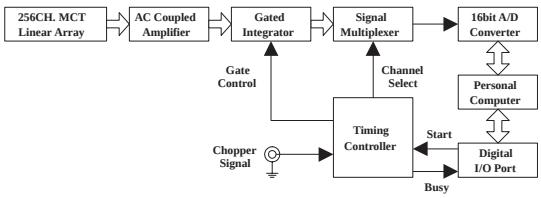

Figure 2. Block diagram of the multi-channel detector system.

Figure 3. Appearance of the multi-channel detector system.

VIII-L-2 Programmable Micro Current Source

Tomonori TOYODA

We have developed a programmable micro current source for growth of conductive organic crystals.

A group of organic crystals are grown by an electrolytic reaction under a constant micro current for a long period of time. The present current source, which can be digitally programmed and controlled, is suitable for such crystal grouth. The appearance of the device is shown in Figure 1. The source shown includes a single module which has eight output channels, and the number of output channels can be increased simply by adding the modules.

Furthermore, based on requests from chemical researchers, the device is equipped with a voltage monitor across both ends of the crystal. This voltage is one of the most important growth parameters since the electrolytic reaction varies according to the voltage. In other current sources, this voltage has not often been utilized to control the crystal growth. In the present device the output current can be controlled so that the voltage across both ends of the crystal under growth does not exceed a certain point. This feature may enable users to isolate crystals in a certain single oxidization (deoxidization) state out of many possible states. The device can also be used to find optimal growth conditions of the crystals by investigating the programmed current profiles.

Figure 1. Appearance of the programmable micro current source.

VIII-M Development of Experimental Devices

VIII-M-1 Prototype Apparatus for Synthesizing the Single Wall Carbon Nanotubes by Arc Discharge at High Temperature Environment

Tatsuharu TORII and Shunji BANDOW *(Japan Science & Technology Corporation)*

The single wall carbon nanotubes (SWNTs) can be synthesized by arc burning of the carbon rod containing bi-metallic catalysts such as Ni-Y, Co-Ni and Fe-Ni. Normally, the composite carbon rod is burnt by arcing at a room temperature environment. Recently, it was found that the synthesis rate of SWNTs was accelerated at high temperature environment (T < ~ 850 °C) by the laser evaporation method.[1)] Here we designed an apparatus for studying the temperature effect on yielding the SWNTs by the arc vaporization method.

Figure 1 is a schematic of the apparatus for arc vaporization of the composite carbon rod at high temperature. The composite carbon rod (10 mm in diameter) is set at the end of the positive electrode and the counter rod is pure carbon (number 3 in Fig. 1), both of which are set in the quartz tube(50 mm in diameter and 1000 mm in length, number 1 in Figure 1). The environment temperature around the arcing is controlled by a 300 mm electric tube furnace placed near the center of the quartz tube, whose furnace can elevate the temperature up to 1200 °C. The part number 2 in Figure 1 is a handle for feeding a composite carbon rod to adjust a spark gap. Most of the SWNTs prepared under high temperature environment are carried by the He flow (500 Torr,100 sccm) and gathered on the water cooled copper collector. The photographic picture of this apparatus is shown in Figure 2.

It is also planned for further study to construct an automatic spark gap adjusting system to realize a suitable sparking condition.

Reference

1) S. Bandow, et al., Phys. Rev. Lett. 80, 3779 (1998).

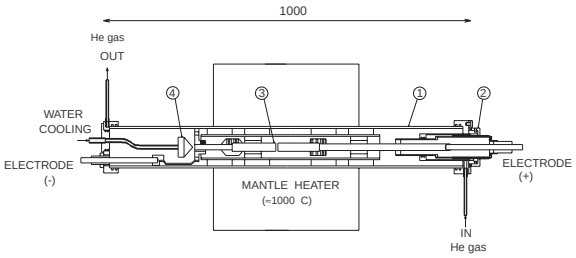

Figure 1. Schematic of the apparatus for arc vaporization of the composite carbon rod at high temperature.

Figure 2. Photographic picture of the apparatus.

VIII-N Development of Spectroscopic System with Combination of Synchrotron Radiation and Laser

VIII-N-1 Time-Gated Photon Counting Method for Two-Photon Spectroscopy Using Synchrotron Radiation and Laser

Shuji ASAKA, Shunsuke NAKANISHI *(Kagawa Univ.)*, **Hiroshi ITOH** *(Kagawa Univ.)*, **Masao KAMADA** *(UVSOR Facility)*, **Masayuki WATANABE** *(Kyoto Univ.)*, **Osamu ARIMOTO** *(Okayama Univ.)*, **Shigeki FUJIWARA** *(Okayama Univ.)*, **Toru TSUJIBAYASHI** *(Osaka Dental Univ.)* **and Minoru ITOH** *(Shinshu Univ.)*

[*Rev. Sci. Instrum.* **69**, 1931 (1998)]

A new measurement system has been developed for two-photon spectroscopy in solids with a combination of synchrotron radiation and laser. This system is based on a time-gated photon counting technique (Figure 1) to observe luminescence signals induced by two-photon excitation. It is demonstrated that this technique enables us to achieve a high sensitivity and a good signal-to-noise ratio because it is a kind of zero-method.

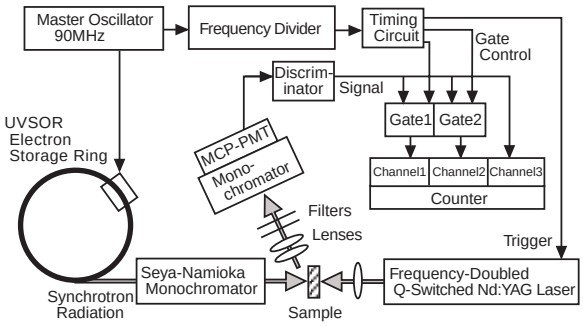

Figure 1. Block diagram of experimental setup for two-photon spectroscopy.

Ultraviolet Synchrotron Orbital Radiation Facility

VIII-O Development of the UVSOR Light Source

VIII-O-1 Non-linear Calibration of Beam Position Monitors

Masahito HOSAKA, Shiro TAKANO *(SPring-8)*, **Jun-ichiro YAMAZAKI, Toshio KINOSHITA, Hitoshi TANAKA** *(SPring-8)* **and Hiroyuki HAMA**

To deduce higher order terms of the dispersion function in the UVSOR storage ring by measuring slight changes of the beam equilibrium orbit, precise calibrations of the beam position monitors (BPMs) are crucial. A first order form of the solution of the Poisson equation for a vacuum chamber at the BPMs has been used so far. However there was a couple of difficulties and problems; (1) a very narrow region to be properly applied (< 3 mm) and (2) attenuation due to connectors and cables were not exactly known, so that experimental data derived from the BPMs has been less accuracy and reliability. To overcome these issues, a numerical evaluation for inductive electric fields in the chamber has been performed by using a boundary element method and a higher order expansion of the analytical solution of the Poisson equation up to 10-th order has been also evaluated. Both results are quite in good agreement in a very wide range (< 10 mm). Attenuation factors for all button monitors were obtained by using a least squares method to fit an identical position deduced from four different combinations of three button monitors in a BPM. Consequently the accuracies of the beam position of 5 μm and 10 μm for the horizontal and the vertical planes, respectively, were obtained.

VIII-P Researches by the USE of UVSOR

VIII-P-1 Time Response and Temperature Dependence of Photo-Stimulated Desorption of Sodium Atoms from Sodium Halides

Sayumi HIROSE *(Sumitomo Heavy Industries Ltd.)* **and Masao KAMADA**

[*J. Electron Spectroscopy and Related Phenomena* **92**, 109 (1998)]

Photo-stimulated desorption (PSD) of sodium atoms from sodium halide crystals has been investigated using intense synchrotron radiation from a planar-type undulator. The PSD intensities of ground-state and excited-state Na atoms showed different temperature dependence, indicating different desorption processes. The temperature dependence of the PSD intensities was also different from that of thermally-stimulated desorption. Moreover, time response of the excited-state Na desorption was found to consist of a nano-second component and a slower one. The temperature dependence of the nano-second component was also different from that of the slow PSD. These present results are consistent with the idea that the excited-state alkali desorption can be interpreted with two models, a fast desorption induced by electronic transition in the surface layer and a slow one due to thermal process of surface defects.

VIII-P-2 Laser-Induced Fluorescence Study of Fast Desorption of Ground-State K Atoms from Potassium Halides Excited by Synchrotron Radiation

Masao KAMADA and Sayumi HIROSE *(Sumitomo Heavy Industries Ltd.)*

[*Surface Science* **390**, 194 (1997)]

The nano-second desorption of ground-state K atoms from KCl was investigated for the first time by using a laser-induced fluorescence method with synchrotron radiation and laser pulses. It was found that the desorption consists of a nano-second component and a slow one more than 178 ns. The fast desorption is several orders of magnitude faster than the existing results of the time response of ground-state alkali desorption. Therefore, the fast desorption of ground-state alkali atoms can not be interpreted with the existing mechanisms and requires a new desorption model. We suggest that the lattice instability due to the electronic excitation in the surface layer may play an important role on the fast desorption of ground-state alkali atoms.

VIII-P-3 Circular Dichroism in the Angular Distribution of Core-Level Photoelectrons from GaAs (111)

Masao KAMADA, Yong Q. CAI *(Univ. Tokyo)*, **Naoshi TAKAHASHI** *(Heinrich-Heine-Univ. Duesseldorf)*, **Shin-ichiro TANAKA and D. A. WOOLF** *(Univ. Wales, UK)*

[*J. Electron Spectroscopy and Related Phenomena* **72**, 219 (1998)]

The circular dichroism of angle-resolved photoelectron spectra was investigated for core-levels from clean and hydrogen exposed GaAs (111) surfaces. It was found that the circular dichroism of Ga-3d and As-3d photoelectrons shows clear dependence on the emission angle of the photoelectrons and the sample surface. It is proposed that the experimental results may be interpreted primarily in terms of the interference of photoelectrons affected by the anisotropic field in the surface layer of GaAs (111).

VIII-P-4 Simultaneous Measurements of Photoelectron and Luminescence of Barium Halides

Masao KAMADA, Shigeki FUJIWARA *(Okayama Univ.)*, **Osamu ARIMOTO** *(Okayama Univ.)*, **Yasuo FUJII** *(Osaka City Univ.)* **and Shin-ichiro TANAKA**

[*J. Electron Spectroscopy and Related Phenomena* **88-91**, 297 (1998)]

Photoelectron and optical spectra are both important to know the electronic structures of solids, but they have been measured independently in insulating materials so far. In the present experiments, simultaneous measurements of photoelectron and luminescence spectra of BaF2 thin films were carried out. It was found that both photoemission and luminescence intensities decrease with increasing synchrotron-radiation doses, indicating the formation of radiation-induced defects. Also, the time-correlation between Ba-4d photoelectrons and Auger-free luminescence photons was observed for the first time, suggesting that these correlate with each other.

VIII-P-5 Temperature Dependence of Auger-Free Luminescence in Alkali and Alkaline-Earth Halides

Minoru ITOH *(Shinshu Univ.)*, **Masao KAMADA and Nobuhito OHNO** *(Osaka Electron-Communication Univ.)*

[*J. Phys. Soc. Jpn.* **66**, 2502 (1997)]

Auger-free luminescence (AFL) resulting from a radiative transition between the outermostcore bands and the valence in BaF2, RbF, CsF, CsCl and been studied in a wide range of temperatures from 10 to 300 K. The AFL spectra are separated from those originating from the valence-band excitation with use of time-resolved luminescence spectroscopy. It is found that the decay profile of AFL in each crystal is essentially the same throughout the spectrum. The remarkkable thermal broadening of the linewidth is verilied for all systems. This strongly suggests that the core hole generated on a positive ion induces considerable displacement of the surrounding ions within its lifetime. Based on the predent results, the spectral shape of AFL is discussed in terms of a cluster model and a two-band model, requiring further development of the investigations in theory and experiment.

VIII-P-6 Combinational Use of Synchrotron Radiation and Laser for Two-Photon Spectroscopy of BaF_2[1]

Osamu ARIMOTO *(Okayama Univ.)*, **Shigeki FUJIWARA, Toru TSUJIBAYASHI** *(Osaka Dental Univ.)*, **Masayuki WATANABE** *(Kyoto Univ.)*, **Minoru ITOH** *(Shinshu Univ.)*, **Shunsuke NAKANISHI** *(Kagawa Univ.)*, **Hiroshi ITOH** *(Kagawa Univ.)*, **Shuji ASAKA and Masao KAMADA**

[*J. Electron Spectroscopy and Related Phenomena* **88-91**, 219 (1998)]

We have carried out nonlinear spectroscopy by making use of tunable VUV ligt from synchrotron radiation (SR) together with intense lgt from a laser. The valence excitons of BaF2 with a large band gap of ~11 eV were chosen as our target. A single crystal of BaF2 was irradiated at 15 K by the two light pulses from the SR (6-9eV) and an Nd:YAG laser (2.33eV). Self-trapped exciton luminescence induced by two-photon excitation was detected with a time-gated photon-counting system developed for the present study. This zero-method technique is expected to be sensitive compared to early experiments by an Italian group monitoring transmittance changes. The energy of the 2P exciton is estimated to be 10.6 eV at 15 K.

VIII-P-7 Direct Excitation of Tl^+ Impurity Ions by Hot Photoelectrons in Wide-Gap Crystals

E. FELDBACH *(Inst. Physics)*, **Masao KAMADA, M. KIRM** *(Inst. Physics)*, **A. LUSHCHIK** *(Tartu Univ. and IMS)*, **Ch. LUSHCHIK** *(Inst. Physics)* **and I. MARTINSON** *(Lund Univ.)*

[*Phys. Rev. B* **56**, 13908 (1997)]

The reflection spectra of KCI and RbCl crystals and excitation spectra of *A* and *B* luminescence and recombination phosphorescence of Tl^+ centers for RbCl:Tl and KCl:Tl crystals have been measured in a spectral region from 5 to 30 eV. The energy distribution curvers of emitted electrons have been measured on the excitation of RbCl thin films by 13-30 eV photons. The comparative analysis of optical and photoelectric characteristics allowed us to reveal the effect of direct excitation of Tl^+ impurity ions up to *A* ($^3P_1$), *B* ($^3P_2$), and *C* ($^1P_1$) states by hot conduction electrons. The threshold photon energies of this effect are determined. The estimated energies of conduction electrons, formed by such photons, are close to the energies of direct optical transitions $^1S_0 \rightarrow {}^3P_1$ (5 eV) and $^1S_0 \rightarrow {}^3P_2$ (6eV) of Tl^+ centers in KCl:Tl and RbCl:Tl crystals. Similar to the case of ns^2 free atoms, the excitation functions for triplet states of Tl^+ centers have a sharp maximum at the energy just above the threshold in RbCl:Tl and KCl:Tl crystals. The peculiarities of electron impact spectroscopy of impurity ions in wide-gap crystals are discussed.

VIII-P-8 Study of Ion Desorption Induced by the Core-Level Excitation on the CaF_2(111) Surface

Shin-ichiro TANAKA, Kazuhiko MASE, Mitsuru NAGASONO and Masao KAMADA

[*J. Elec. Spec. and Rel. Phenom.* **92**, 119 (1998)]

Desorption of F^+ induced by core-level excitation with synchrotron radiation has been investigated on the

CaF_2 (111) film produced on Si(111). The ion yield is proportional to electron yield in the region of Ca-2p edge, while an enhancement of the ion yield is observed at the photon energy for the F-1s core-exciton. The peak corresponding to the F-1s excitation observed in the ion yield is shifted from that in the electron yield by about -1.2eV, which is predominantly ascribed to the change in the Madelung potential at the surface. The electron-ion coincidence study shows that the F^+ desorption is directly stimulated via a decay of the F-1s surface core-exciton, while secondary-electron stimulated desorption is the predominant process after the creation of Ca-2p hole.

VIII-P-9 Observation of the Surface States on CuCl(100)

Shin-ichiro TANAKA and Masao KAMADA

[*J. Elec. Spec. and Rel. Phenom.* **88-91**, 689 (1998)]

The surface electronic structure of the CuCl(100) film produced on the Si(100) surface was investigated by using the angle-resolved photoelectron spectroscopy with synchrotron radiation. Two surface states were observed, and assigned to Cl-3p and Cu-3d, respectively. The dispersions of them were measured (Figure 1). The photoelectron spectra of the CuCl(100) surface exposed to CO gas were also observed, and it was found that CO is adsorbed on CuCl(100) through a Cu atom.

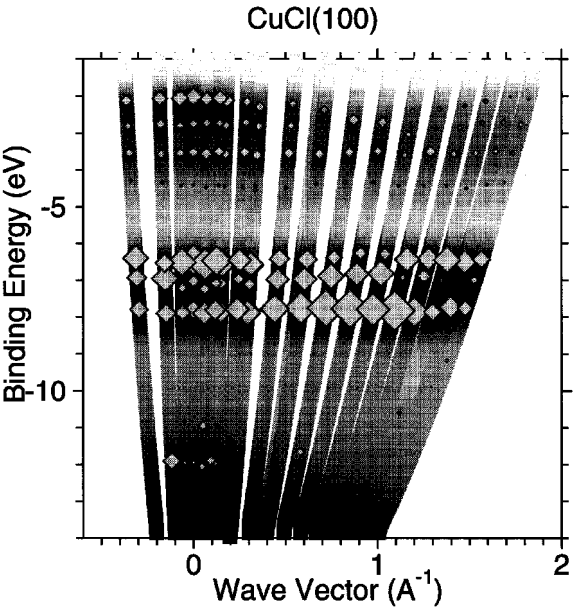

Figure 1. Band dispersions determined by angle resolved photoelectron spectroscopy. Grey tapes correspond to photoelectron spectra. Symbols correspond to the components of fitting calculations, and their size indicates the area intensity of components.

VIII-P-10 Electronic Structures of Organic Salts (DI-DCNQI)$_2$M (M = Cu and Ag) Using Photo-electron Spectromicroscopy

Yuichi HARUYAMA, Shin-ichi KIMURA, Yüksel UFUKTEPE *(Univ. Cukurova-Turkey)***, Toyohiko KINOSHITA, Krishna Gopal NATH, Ko-ichi HIRAKI** *(Gakushuin Univ.)* **and Kazushi KANODA** *(Univ. Tokyo)*

The electronic structures of organic salts (DI-DCNQI)$_2$M with M = Cu and Ag, where DI-DCNQI is 2,5-diiodo-N,N'-dicyanoquinonediimine, have been studied at various photon energies using the photo-electron spectromicroscopy. The experiments have been performed at the BL5B with VG ESCALAB 220i-XL system. From the photon energy dependence of the photoionization cross-section, the atomic orbital characters of the observed spectral features are determined. For both (DI-DCNQI)$_2$Cu and (DI-DCNQI)$_2$Ag, the C and N 2*p* states originating in the cyano group and the quinone ring are located at ~ 4.0 eV and ~ 6.5 eV, respectively. The Cu 3*d* states for (DI-DCNQI)$_2$Cu and the Ag 4*d* states for (DI-DCNQI)$_2$Ag are located at ~ 3.5 eV and ~ 5.5 eV, respectively. This indicates that the *p*π-*d* hybridization at the Fermi level between the M ions and the N atoms of the DCNQI columns is larger for (DI-DCNQI)$_2$Cu than for (DI-DCNQI)$_2$Ag. From the comparison between the observed photoemission spectra for (DI-DCNQI)$_2$Cu and the previous ones for (DMe-DCNQI)$_2$Cu,[1] the energy shifts of the C and N 2*p* states originating in the quinone ring and the Cu 3*d* states are observed. These energy shifts probably reflect the difference in the chemical bond caused by the minor structural change.

Reference

1) A. Tanaka, A. Chainani, T. Miura, T. Takahashi, T. Miyazaki, S. Hasegawa and T. Mori, *Solid State Commun.* **93**, 1 (1995).

VIII-P-11 Resonant Photoemission Study of Temperature-Induced Valence Transition Material $EuNi_2(Si_{1-x}Ge_x)_2$

Heralu Pathirannehelage Nihal Jayalath GUNASEKARA *(Ceylon Inst. Sci. and Ind. Research, Sri Lanka)***, Yasutaka TAKATA, Shin-ichi KIMURA, Toyohiko KINOSHITA, Nobuhiro KOSUGI, Krishna Gopal NATH, Hirofumi WADA** *(Kyoto Univ.)***, Akihiro MITSUDA** *(Kyoto Univ.)***, Masayuki SHIGA** *(Kyoto Univ.)***, Haruhiko OGASAWARA** *(Univ. Tokyo)* **and Akio KOTANI** *(Univ. Tokyo)*

Among the intermediate valent systems of rare earth compounds, Eu compounds are known to exhibit strong temperature dependence of the mean valence. Very recently, it was found that the $EuNi_2(Si_{1-x}Ge_x)_2$ compounds with $0.70 \leq x \leq 0.82$ show a temperature induced valence transition below room temperature.[1] It has been known that the 3*d*-4*f* resonant photoemission of such kind of mixed valent 4*f* compounds is a rather useful technique to clarify the different 4*f* electronic states owing to different valence than the 4*d*-4*f* resonant photoemission. In this study, we have applied the 3*d*-4*f* resonant photoemission method to investigate the valence transition of the $EuNi_2(Si_{1-x}Ge_x)_2$ compound. The experiments were performed at BL1A with the SCIENTA SES-200 analyzer. Figures show the

resonant photoemission spectra along with the photoelectron total yield (TY) spectra around the Eu 3*d*-4*f* excitation region at about 300K and 80K. It is noticed that the peaks 2 and 3 for the TY spectrum are enhanced at the low temperature phase. This is due to the increase of the trivalent Eu ion component at low temperature. In the same manner, the trivalent components of Eu 4*f* photoemission states are enhanced at the excitation conditions of 2 and 3, whereas the divalent 4*f* states are dominant at 1, 4 and 5. From these results, the features around 0-4 eV binding energy are estimated to be mostly divalent 4*f* states and those around 6-12 eV are trivalent ones in these on-resonant spectra.The results were compared with the theoretical calculation based on an atomic model for divalent and trivalent Eu ions. The estimated values of the mean valence for both temperature were smaller than those reported before. This may be due to the effect of the oxidization of the samples in the previous experiments.[1)]

Reference

1) H. Wada, A. Nakamura, A. Mitsuda, M. Shiga, T. Tanaka, H. Mitamura and G. Goto, *J. Phys., Condens. Matter.* **9**, 7913 (1997).

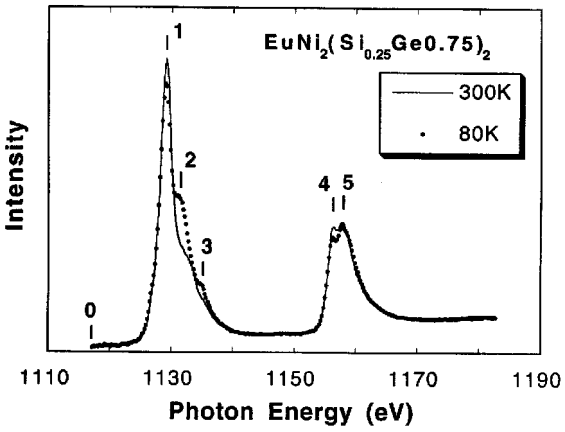

Figure 1. 3*d*-4*f* TY spectra for $EuNi_2(Si_{1-x}Ge_x)_2$ (x = 0.75) at 300K and 80K.

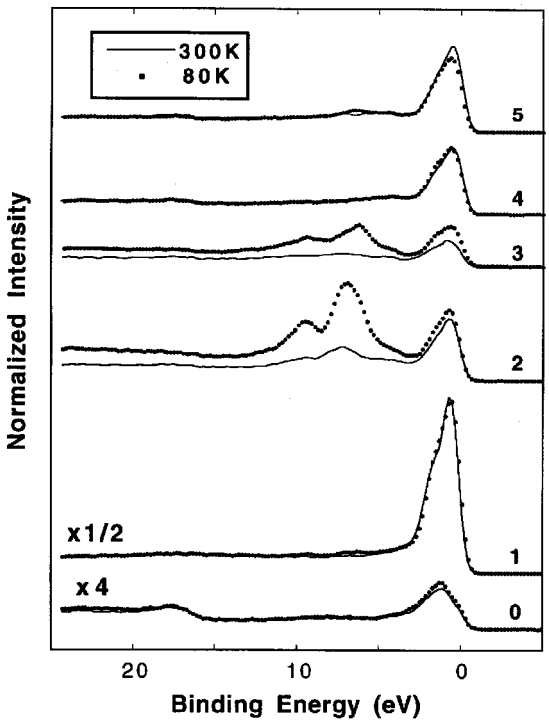

Figure 2. 3*d*-4*f* Resonant photoemission spectra for $EuNi_2(Si_{1-x}Ge_x)_2$ (x = 0.75).

VIII-P-12 Study of Magnetic Linear Dichroism (MLD) for Different Thickness of Ni-Thin Film Grown on Ferromagnetic Co (100) in Element Specific Photoemission

Krishna Gopal NATH, Yuichi HARUYAMA, Shinichi KIMURA, Yüksel UFUKTEPE *(Univ. Cukurova-Turkey)* **and Toyohiko KINOSHITA**

Study of the thin film magnetism is one of the expanding topics in the surface science. In order to investigate the magnetic behaviors of Ni/Co (100) and compare with those of Ni/Cu (100), we measured magnetic linear dichroism (MLD) for either the valence band or the core level (3*p*) photoelectrons of the different thickness of Ni-film grown on Co substrate. The VG ESCALAB 220i-XL system was connected to the beam line BL5B for the experiments. Thin film is magnetized along two orthogonal directions in the surface plane (in-plane magnetization) where one of these directions is along Cu [100] direction.

Figure 1 shows the MLD results for 3d bands of the Ni thin films on Co and Cu substrates, respectively, taken at the photon energy of 67.2eV, i.e. the Ni 3*p*-3*d* resonant condition. It is found in Figure 1(a) that both the main peak ($3d^9$) and the satellite peak ($3d^8$) show asymmetry but in opposite sign from each other for Ni/Co system. On the other hand, the Ni/Cu system does not show the MLD. This is an evidence that the Ni thin film around 10ML on Co shows in-plane magnetization at room temperature whereas the Ni/Cu does not show the in-plane magnetization. The MLD results in Figure 1(a) is similar to the previous MCDAD result but not similar to the MLDAD result reported by Ueda et al.[1)] The theoretical calculation is in progress, which will give us more clear understanding about resonant

effect on MLD for satellite region.

Reference

1) S. Ueda, S. Imada, Y. Saitoh, T. Mura, M. Kasashima, A. Kimura, A. Kakizaki and S. Suga, *J. Electron Spectrosc. Relat. Phenom.* **88-91**, 191 (1998).

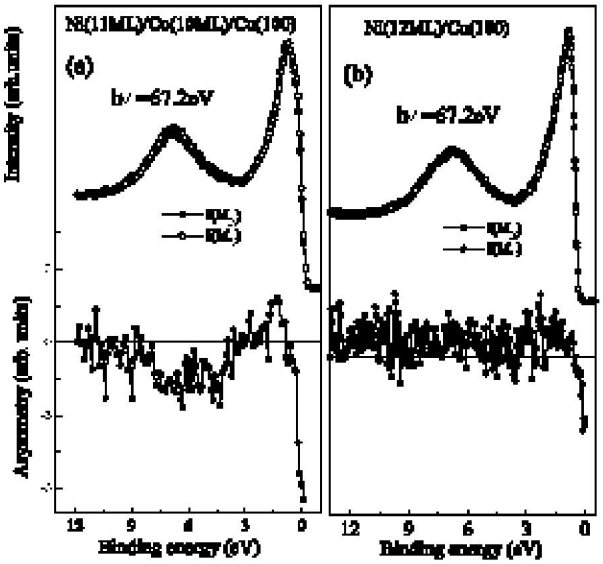

Figure 1. Ni 3*d* photoemission spectra for the two magnetized directions **M**//**E**(closed) and **M** **E**(open), where **M** is the vector of magnetization and **E** is of polarization of the light. The lower panel shows the MLD, i.e., asymmetry obtained from the two spectra. (a) is for Ni/Co system and (b) for Ni/Cu.

VIII-P-13 Tm5p Resonant Photoemission Study of TmX (X=S, Se and Te) around 4d-Excitation Region

Krishna Gopal NATH, Yüksel UFUKTEPE *(Univ. Cukurova-Turkey)***, Shin-ichi KIMURA, Toyohiko KINOSHITA, Takeshi MATSUMURA** *(Tohoku Univ.)***, Takashi SUZUKI** *(Tohoku Univ.)***, Haruhiko OGASAWARA** *(Univ. Tokyo)* **and Akio KOTANI** *(Univ. Tokyo)*

In the 4*d*-4*f* resonant process of rare earth compounds, study of resonant behavior of core levels (5*p* or 5*s*) is important to understand overall decay processes related to different electronic states. In fact, the core level photoemission spectra in rare earth systems show complex multiplet structures due to existence of unfilled and localized 4*f*-shell.[1)] Sometimes it is rather difficult to separate the spin-orbit peaks and the valence components if the system is mixed-valence. Followed by the recent resonant photoemission of 4*f*-states at the 4*d*-4*f* excitation condition of thulium compounds (TmS, TmSe, and TmTe) for divalent and trivalent Tm-ions,[2)] in this study, we present the Tm-5*p* photoemission results at the 4*d*-4*f* absorption edges (hν = 150-200 eV) of Tm-compounds. The experiments were performed at BL2B1.

Figure 1 shows the on- and off- resonant 5*p* resonant photoemission results of mostly divalent compounds TmTe. It is noticed that the resonance effect is larger for higher binding energy states, i.e. around 30 eV than lower ones around 24 eV. In Figure 2, the resonance behavior of trivalent Tm5*p* of TmSe, a typical mixed-valent compound, is shown. The photoemission spectra also show the both Tm^{3+} and Tm^{2+} components as seen in the comparison with the calculated curves for two valences. It is found that 4*d*5*p*4*f*-decay channel is also active but not so strong as 4*d*4*f*4*f* decay channel. The photoemission spectra for two Tm-valences are defined by complex multiplet structures, not only by single 5*p*3/2 or 5*p*1/2 peak.

References

1) A.Kotani, *Inner shell photoelectron process in solids* (Hand book on synchrotron Radiation), vol. 2, G. V. Marr, Ed., North-Holland Physics Publishing; Amsterdam (1987).
2) Y.Ufuktepe, S. Kimura, T. Kinoshita, K. G. Nath, H. Kumigashira, T. Takahashi, T. Matsumura, T. Suzuki, H. Ogasawara and A. Kotani, *J. Phys. Soc. Jpn.* **67**, 2018 (1998).

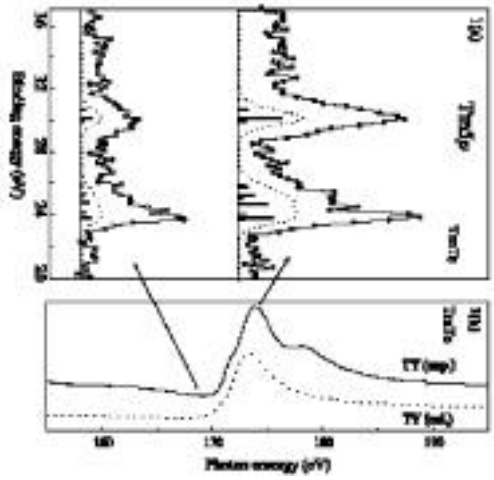

Figure 1. (a) On (upper)- and off (lower)-resonant photoemission spectra of Tm5*p* for TmTe, mostly divalent compounds. The calculated spectra for Tm divalent ion are shown for comparison.
(b) Photoelectron total yield spectrum of TmTe around the Tm4*d* edge. The calculated spectrum for Tm divalent ion is also shown.

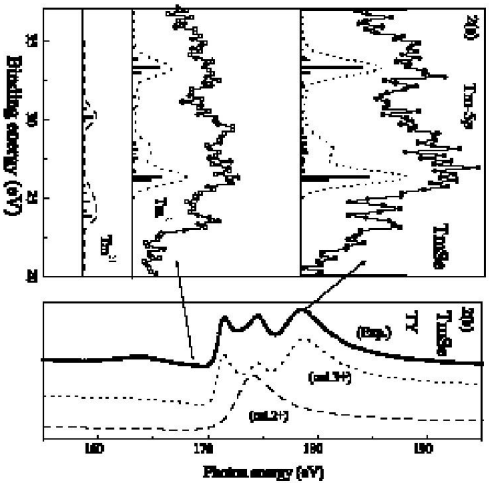

Figure 2. Same as in Figure 1, but for TmSe. Both the divalent and trivalent components are observed and calculated.

VIII-P-14 Photodissociation of Ozone in the K-Edge Region

Tatuso GEJO, Kazumasa OKADA *(Hiroshima Univ.)*, **Toshio IBUKI** *(Kyoto Univ. Education)*, **Norio SAITO** *(ETL)* **and Isao H. SUZUKI** *(ETL)*

Ozone is one of the most important molecules in chemistry since ozone in the stratosphere absorbs UV light emitted from the sun and prohibits humanity from the exposure by the UV light. We have investigated the photochemistry and photodissociation dynamics of Ozone in K-edge region with angle-resolved time-of-flight apparatus for the first time. TOF spectra were obtained at 0 and 90 degree relative to the axis of soft x-ray polarization. At π^* excitation from 1s level of terminal ones, O^+ and O_2^+ photofragments are observed to be emitted to the direction perpendicular to the polarization of light, which is consistent with our assignment.[1] TOF spectra at π^* excitation from that of center one, however, shows more isotropic ones. It suggests the overlap of several electronic states. This is consistent with our calculation which predict that π^* state ($2b_1$) are overlapped with σ^* ($5a_1$) state in this band. A π^* excitation from inner-1s of center oxygen atom generates preferably O^+, compared to that from inner-1s of terminal oxygen atoms.

Reference

1)T. Gejo, K. Okada and T. Ibuki, *Chem. Phys. Letters* **277** 497 (1997)